

University of Montana

ScholarWorks at University of Montana

Graduate Student Theses, Dissertations, &
Professional Papers

Graduate School

1999

Evaluation of spectrophotometric pH methods for freshwater measurements

Craig M. French
The University of Montana

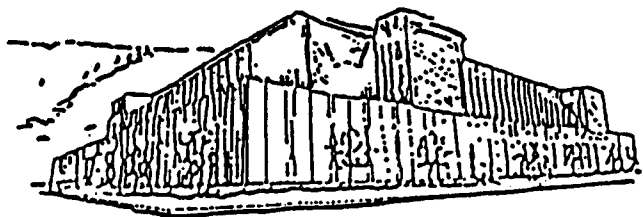
Follow this and additional works at: <https://scholarworks.umt.edu/etd>

Let us know how access to this document benefits you.

Recommended Citation

French, Craig M., "Evaluation of spectrophotometric pH methods for freshwater measurements" (1999).
Graduate Student Theses, Dissertations, & Professional Papers. 2256.
<https://scholarworks.umt.edu/etd/2256>

This Thesis is brought to you for free and open access by the Graduate School at ScholarWorks at University of Montana. It has been accepted for inclusion in Graduate Student Theses, Dissertations, & Professional Papers by an authorized administrator of ScholarWorks at University of Montana. For more information, please contact scholarworks@mso.umt.edu.



Maureen and Mike
MANSFIELD LIBRARY

The University of **MONTANA**

Permission is granted by the author to reproduce this material in its entirety,
provided that this material is used for scholarly purposes and is properly cited in
published works and reports.

*** Please check "Yes" or "No" and provide signature ***

Yes, I grant permission

No, I do not grant permission

Author's Signature Craig Farnel

Date 5/17/99

Any copying for commercial purposes or financial gain may be undertaken only with
the author's explicit consent.

**EVALUATION OF SPECTROPHOTOMETRIC pH METHODS FOR
FRESHWATER MEASUREMENTS**

By

Craig M. French

B.S. Eastern Illinois University, 1993

presented in partial fulfillment of the requirements

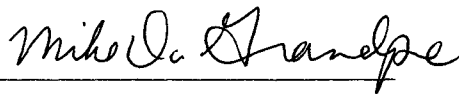
for the degree of

Master of Science

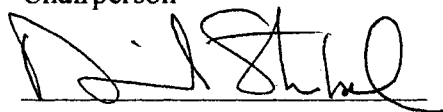
The University of Montana

1999

Approved by



Chairperson



Dean, Graduate School

5/17/99

Date

UMI Number: EP33862

All rights reserved

INFORMATION TO ALL USERS

The quality of this reproduction is dependent on the quality of the copy submitted.

In the unlikely event that the author did not send a complete manuscript and there are missing pages, these will be noted. Also, if material had to be removed, a note will indicate the deletion.



UMI EP33862


Copyright 2012 by ProQuest LLC.

All rights reserved. This edition of the work is protected against unauthorized copying under Title 17, United States Code.



ProQuest LLC.
789 East Eisenhower Parkway
P.O. Box 1346
Ann Arbor, MI 48106 - 1346

Evaluation of Spectrophotometric pH Methods for Freshwater Measurements

Director: Michael D. DeGrandpre 

An autonomous spectrophotometric instrument is being developed for freshwater pH measurements. The instrument operates by recording the absorbances of a thermodynamically characterized indicator (cresol red) mixed with the freshwater sample. Cresol red is a weak acid and therefore perturbs the pH of freshwater samples. The pH perturbation caused by cresol red is evaluated theoretically and experimentally. The instrument consists of a miniature solenoid pump and valve, a fiber-optic flow cell, a low power data logger, and various other easy to acquire optical components. Laboratory experiments were conducted to determine the relative accuracy and precision of the spectrophotometric instrument with buffer solutions and freshwater. Freshwater pH perturbation was reduced by changing from a 0.75 cm to a 2.0 cm pathlength fiber-optic flow cell. The 3σ precision was ± 0.003 pH units and the relative accuracy was ± 0.008 pH units compared to results from an UV-VIS spectrophotometer. Spectrophotometric methods make reproducible pH measurements possible in freshwater.

ACKNOWLEDGMENTS

I would like to give thanks to Mike DeGrandpre for his guidance and support throughout this project. I would like to thank Terry Hammar, who works at the Woods Hole Oceanographic Institution, for the electronics and the fiber-optic flow cells. I would also like to thank all of my co-workers in the DeGrandpre lab for their advice and support. This research was funded by the Department of Energy and the National Science Foundation. Last but not least, I would like to give thanks to my parents, Gene and Sheri French, who provided support and encouragement throughout my academic pursuits.

TABLE OF CONTENTS

Abstract	ii
Acknowledgments	iii
Table of Contents	iv
List of Tables	vi
List of Figures	vii
CHAPTER 1: INTRODUCTION	1
CHAPTER 2: OPERATING PRINCIPLES	
2.1 Theory of the Byrne Method	7
2.2 The Byrne Method	9
CHAPTER 3: METHODS	
3-A.1 Characterization of the Indicator	11
3-A.2 pK_a uncertainties	15
3-A.3 pH perturbation	16
3-A.4 CR Purification	20
3-B Instrument Design	23
3-B.1 Instrument Layout	23
3-B.2 Blank Measurements	29
3-B.3 Evaluation of the Plumbing System	32
3-B.4 Evaluation of the Optical System	33
3-C Relative Accuracy Experiments	35
3-C.1 Buffer Solution Preparation	35
3-C.2 Freshwater Sample Preparation	36
3-C.3 ALpHI Procedure	36
3-C.4 UV-VIS Spectrophotometric pH Measurement Procedure	37
3-C.5 Temperature Compensation	38
CHAPTER 4: RESULTS	
4.1 Buffer Solution Relative Accuracy Experiment	40
4.2 Freshwater Relative Accuracy Experiments	45

CHAPTER 5: DISCUSSION	
5.1 Relative Accuracy	55
5.2 ALpHI Precision	56
5.3 Optimal Response Characteristics of ALpHI	57
5.4 Freshwater pH Perturbation	58
CHAPTER 6: CONCLUSIONS	
6.1 Summary of Results	59
6.2 Future Applications	59
APPENDIX I: DERIVATION OF EQUATION 6.	61
APPENDIX II: CRTURB.BAS	64
APPENDIX III: ALPHI1.TT4	68
REFERENCES	73

LIST OF TABLES

Table 1-1 Literature Review	5
Table 3-1 Molar Absorptivities	12
Table 3-2: Molar Absorptivity Ratios	12
Table 3-3: CR Thermodynamic Properties	14
Table 3-4: pH of Diluted CR Solutions	19
Table 4-1 Freshwater Error with 0.75 cm Cell	49
Table 4-2: Freshwater Error with 2.0 cm Cell	54
Table 5-1 Relative Accuracy Summary	55
Table 5-2: Precision Summary	56
Table 5-3: Optimal Response Characteristics	57

LIST OF FIGURES

Figure 2-1	Absorbance spectra	8
Figure 3-1.	Structure of cresol red	11
Figure 3-2:	Temperature dependence of CR pK_a	15
Figure 3-3:	Theoretical pH perturbation at multiple Alk	18
Figure 3-4	Theoretical pH perturbation at one [CR] with slopes	19
Figure 3-5.	Comparison of theoretical and experimental pH perturbation	20
Figure 3-6:	ALpHI layout	23
Figure 3-7:	Cut away view of the flow cell	25
Figure 3-8:	Analysis of one pulse of indicator	28
Figure 3-9:	Example of one measurement cycle	29
Figure 3-10:	Valve comparison	31
Figure 3-11.	A study of the response time	32
Figure 3-12:	pH temperature compensation	38
Figure 4-1:	Absorbance, temperature, and pH of a buffer solution	41
Figure 4-2:	Correlation between pH and [CR]	42
Figure 4-3:	Results of buffer solution reproducibility experiment.	44
Figure 4-4	Absorbance, temperature, and pH of a freshwater sample with 0.75 cm flow cell.	46
Figure 4-5	Results of freshwater with 0.75 cm flow cell reproducibility Experiment	47
Figure 4-6:	1 1 comparison of the ALpHI pH and UV-VIS spectrophotometer pH with the 0.75 cm flow cell.	49
Figure 4-7:	Absorbance, temperature, and pH of a freshwater sample with 2.0 cm flow cell	51
Figure 4-8:	Results of freshwater with 0.75 cm flow cell reproducibility Experiment	52
Figure 4-9:	1.1 comparison of the ALpHI pH and UV-VIS spectrophotometer pH with the 2.0 cm flow cell	53

Chapter 1

Introduction

pH, defined as $-\log a_{\text{H}^+}$, where a_{H^+} is hydrogen ion activity, is perhaps the most analyzed parameter of freshwater systems. pH is useful for studying the acidification of lakes and rivers (Herczeg and Hesslein 1984, Herczeg et al. 1985, Stauffer 1990a, 1990b; Webb and Sasowsky 1994). pH is also an important parameter in geochemical studies because trace elements undergo pH dependent adsorption-desorption reactions (Fuller and Davis 1989; Brick and Moore 1996). Investigations of the partial pressure of CO_2 ($p\text{CO}_2$), alkalinity, and dissolved inorganic carbon (DIC) also utilize pH measurements (Kratz et al. 1987; Hoffer-French and Herman 1988, Maberly 1996; Raymond et al. 1997).

Although freshwater pH is commonly measured, pH measurements may be highly variable because they are dependent upon many factors. Freshwater pH is primarily controlled by the bicarbonate-carbonate equilibria, therefore any fluctuations in CO_2 affect the CO_2 equilibria and therefore also the pH. Changes in CO_2 can be caused by such factors as biological activity, air-water gas exchange, temperature changes, and groundwater inputs. Photosynthesis, for example, can increase the pH by consuming CO_2 . These factors make grab sampling-based measurements too infrequent to accurately characterize diel, episodic or seasonal pH changes. Other researchers have recognized the need for more frequent pH measurements. For example, a potentiometric in situ sensor was used to measure pH every 15 min over a one-year period in the surface

waters of Esthwaite Water, Cumbria (Maberly 1996). Although this was a step in the right direction, the uncertainty associated with these results was unacceptable.

However, before this discussion of pH measurement methods continues, a few terms must be defined. Terms such as precision, relative accuracy, and true accuracy will be used in this and subsequent chapters. For the following discussions, precision will be defined as the agreement between measurements over a short time period under constant pH conditions. Relative accuracy is used to describe the reproducibility between various methods over extended periods. True accuracy is the error with respect to the true pH value, however, since the true pH value can not be measured (discussed later), it is impossible to quantify the true accuracy. Consequently, various methods of measuring pH will be evaluated by their precision and relative accuracy.

Glass electrodes are most commonly used for measuring freshwater pH. When using electrodes, the operational definition of pH is:

$$\text{pH}_x = \text{pH}_s + \frac{(E_x - E_s)F}{RT \ln 10} \quad (1)$$

where x and s refer to the unknown and the standard, respectively, E_x and E_s represent the potentials of the electrode when submerged in the unknown and standard, T is the temperature in Kelvin, R is the gas constant and F is the Faraday constant. Although pH electrodes have been used extensively for the measurement of freshwater pH, results from electrodes are often not reproducible as shown in a large number of studies (Herczeg and Hesslein 1984, Davison and Woof 1985, Herczeg et al. 1985, Midgley 1987; Stauffer 1990b; Maberly 1996). Potentiometric relative accuracy primarily suffers

from irreproducible liquid-junction potentials. Since high ionic strength buffers used for calibrations do not produce the same liquid-junction potentials as freshwater, the $E_s - E_x$ term from Equation 1 may be incorrect. This error in potentials causes systematic errors in pH that cannot be avoided. Liquid-junctions may also clog over time causing the electrode to drift. Drifts of as much as 0.05 pH units day⁻¹ have been observed (Davison and Woof 1985), with the severity of the drift dependent on the history of the electrode. Periodic calibrations of electrodes are required to compensate for electrode drift. Therefore, a precision of < 0.03 pH units for freshwater samples requires considerable care to obtain. An autonomous instrument would be of great value for freshwater systems; however, potentiometric methods are impractical because of their dependence on calibrations and sensitivity to liquid junction potentials. Our goal is to develop a method for autonomous in situ freshwater pH measurements that can provide superior long-term reproducibility without calibrations

Because electrode measurements are not reproducible and drift, we looked for an alternative method for an autonomous in situ pH instrument. Several alternative methods for measuring freshwater pH have been reported in the literature. Colorimetric pH indicator kits were evaluated and compared to potentiometric methods (Haines et al. 1983). Based on this study colorimetric pH indicator kits are not considered accurate or practical for in situ work. Work with free-diffusion liquid junctions (FDJ) in freshwater has minimized the systematic error of electrodes (Davison and Woof 1985; Harbinson and Davison 1987). Superior reproducibility (± 0.01 pH units) was typically reported when using FDJ's, however FDJ's are not drift free and are too complex for in situ work. Determining freshwater pH theoretically from DIC, $p\text{CO}_2$ and established

thermodynamic constants for the CO₂ equilibria (Millero 1979) have been investigated (Herczeg and Hesslein 1984, Herczeg et al. 1985). This method is not easily adapted to in situ operations because DIC is impractical to measure in the field. A spectrophotometric method for measuring freshwater pH with a multi-dye system has been used in a flow injection instrument (Pia et al. 1990). This study reported a precision (standard deviation) from ± 0.07 to ± 0.14 pH units for a limited number of trials. Based on this study it would appear that freshwater spectrophotometric methods are not precise enough to be used in an in situ instrument.

However, spectrophotometric methods developed for seawater pH have produced exceptional precision and relative accuracy (Roberto-Baldo et al. 1985; Byrne and Breland 1989; Clayton and Byrne 1993; Bellerby et al. 1995). Hereafter this method will be referred to as the "Byrne method". The Byrne method consists of measurements of absorbance ratios of a pH sensitive dye that is added to the sample. Relative accuracy of the Byrne method (± 0.002 pH units) was determined by measuring seawater buffers (Millero et al. 1993). The Byrne method has been employed in several different ways, such as shipboard flow injection and in situ measurements. A precision of ± 0.005 pH units (Bellerby et al. 1995) to ± 0.003 pH units (Waterbury et al. 1996) is typically reported. Spectrophotometric methods developed by Byrne have dramatically improved the reproducibility of seawater pH measurements over that obtained with pH electrodes. Therefore, the Byrne method appears to be the most promising approach to reach our goal. Although the concept of freshwater spectrophotometric pH measurements is not new, it appears that no one else has attempted to adapt the Byrne method for seawater to freshwater.

Table 1-1 summarizes the extensive literature review. Although freshwater potentiometric measurements are common, pH error and precision are not commonly reported. Therefore, the freshwater potentiometric pH error and precision listed in Table 1-1 represent estimates.

Table 1-1. Literature review summary

Sample	Method	pH error	Precision	Reference (examples)
Seawater	Potentiometric	± 0.02 pH unit	± 0.003 pH unit	Fuhrmann and Zirino 1987
Seawater	Potentiometric	± 0.002 pH unit	± 0.0003 pH unit	Clayton and Byrne 1993
Freshwater	Spectrophotometric	± 0.1 pH unit	± 0.01 pH unit	100's of papers
Freshwater	Spectrophotometric	?	?	Few

A long-term goal of this work is to deploy an in situ pH instrument with the in situ $p\text{CO}_2$ instrument previously developed by DeGrandpre et al. (1995). The resulting data set of pH and $p\text{CO}_2$ would provide a means to calculate DIC and alkalinity, two useful parameters for studying carbon cycling in any water system. These calculations use dissociation constants of carbonic acid and water (Millero 1979). However, a pH relative accuracy of ± 0.1 pH units, as in the Maberly study (1996), will propagate to $\pm 23\%$ uncertainty in the calculated DIC, while a pH relative accuracy of ± 0.01 pH units will decrease the DIC uncertainty to $\pm 2\%$. Larger calculated DIC uncertainties would hinder the ability to resolve the diel DIC cycle of freshwater systems. Therefore, our

objective is to adapt the Byrne method to autonomous in situ freshwater pH measurements with a precision of at most ± 0.005 pH units and a relative accuracy of no greater than ± 0.01 pH units.

The following chapters will be dedicated to describing the theory and nuances of adapting the Byrne method to freshwater pH measurements. Initially, we characterized the molar absorptivity and pK_a of an appropriate indicator. Once an indicator was evaluated, we began designing an automated lab spectrophotometric pH instrument. The timing of the system, plumbing design, and optical layout all required a considerable effort to optimize their performance before the precision and relative accuracy could be determined. The feasibility of an autonomous spectrophotometric pH instrument will be evaluated by determining its precision and relative accuracy compared to an UV-VIS spectrophotometer

Chapter 2

Operating Principle

2.1 Theory of the Byrne Method

The theory behind the Byrne method is based on the dissociation of a weak acid indicator. The equilibrium of a pH indicator, shown in Equation 2, is reached rapidly and use of this equilibrium has proven effective for seawater pH measurements (Robert-Baldo et al. 1985). The equilibrium reaction and its corresponding thermodynamic expression are:



$$K_a = \left(\frac{[\text{H}^+][\text{L}^{2-}]}{[\text{HL}^-]} \right) \left(\frac{\gamma_{\text{H}^+} \gamma_{\text{L}^{2-}}}{\gamma_{\text{HL}^-}} \right) \quad (3)$$

where [] denotes concentration, H^+ represents hydrogen ions, L^{2-} is the unprotonated (base) form of the indicator, HL^- is the protonated (acid) form of the indicator, and γ represents the ion activity coefficients. The most commonly used indicators are the diprotic sulfonephthalein-type. Since the first dissociation reaction of the diprotonated form of the indicator, H_2L , has a $\text{p}K_a$ of approximately 1 to 2, H_2L is not present at the expected pH of the samples (approximately pH 8). Therefore, only the second dissociation constant is important, referred to as K_a in Equation 3

The acid and base forms of sulfonephthalein indicator dyes have well separated wavelength maxima that provide a means to determine their concentrations. However,

determination of exact concentrations of the acid and base species is not necessary to determine pH. Beer's Law and the Henderson-Hasselbalch equation (the log form of Equation 3):

$$A_{\lambda} = \epsilon_{\lambda}bc \quad (4)$$

$$\text{pH} = \text{pK}_a + \log\left(\frac{[\text{L}^{2-}]}{[\text{HL}^{-}]}\right) + \log\left(\frac{\gamma_{\text{L}^{2-}}}{\gamma_{\text{HL}^{-}}}\right) \quad (5)$$

where A_{λ} is the absorbance at a given wavelength, ϵ_{λ} is the molar absorptivity at a given wavelength, b is the optical pathlength in cm, and c is the indicator acid or base concentration, are used to derive an equation that allows calculations of pH as a function of the ratio of base and acid absorbances (spectra are shown in Figure 2-1).

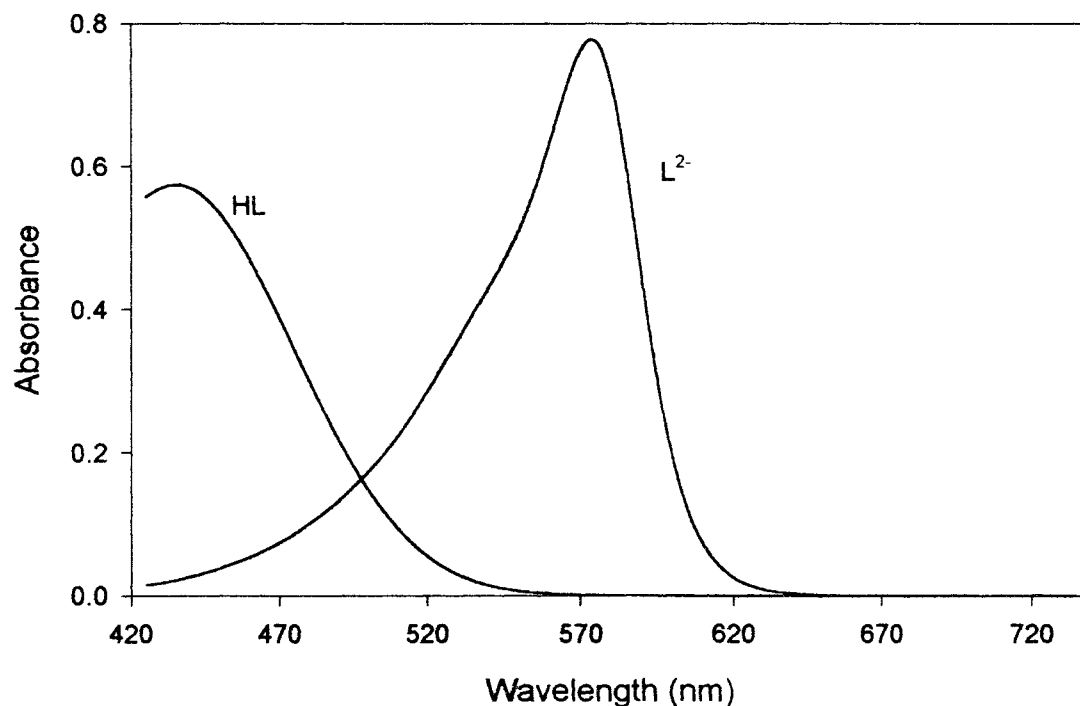


Figure 2-1. Absorbance spectra of L^{2-} and HL are shown for the pH indicator cresol red. Spectra were obtained on the UV-VIS spectrophotometer at pH ≈ 12 (L^{2-}) and pH ≈ 4.5 (HL) with $[\text{L}^{2-}] = 1.622 \times 10^{-6}$ M and $[\text{HL}] = 2.662 \times 10^{-6}$ M

pH can be determined by spectrophotometric measurements using the following equation derived from Equations 4 and 5 (Clayton and Byrne 1993):

$$\text{pH} = \text{pK}_a + \log \left(\frac{R - e_1}{e_2 - R e_3} \right) \quad (6)$$

where R is the absorbance ratio, $R = A_{577} / A_{439}$, of the base form absorbance (A_{577}) to the acid form absorbance (A_{439}) and e_i are the molar absorptivity ratios:

$$e_1 = \frac{\epsilon_{a577}}{\epsilon_{a439}} \quad e_2 = \frac{\epsilon_{b577}}{\epsilon_{a439}} \quad e_3 = \frac{\epsilon_{b439}}{\epsilon_{a439}} \quad (7)$$

where ϵ is the molar absorptivities of either the acid (a) or base (b) form of the indicator. The complete derivation of Equation 6 is located in Appendix I. Therefore the ratio of indicator species, $[L^{2-}] / [HL^-]$, is expressed in terms of R and e_i . R is determined from absorbance measurements at multiple wavelengths:

$$A_\lambda = -\log \left(\frac{I_\lambda}{I_o} \right) \quad (8)$$

where A_λ is the indicator absorbance, I_λ is the transmitted light intensity at an absorbing wavelength (439 or 577 nm), and I_o is the transmitted intensity of the blank at λ .

2.2 The Byrne Method

Seawater spectrophotometric pH measurements were obtained by Byrne and Breland (1989) in the following four-step procedure: 1. A 10 cm spectrophotometric cell was flushed with 150 – 250 ml of seawater before being sealed with no air space. 2. The

cell was warmed to 25.0°C in a thermocirculator bath. 3 After drying and cleaning the optical surfaces, the cell was placed in the sampling compartment of a spectrophotometer. Measurements of baseline absorbances at the acid, base and reference wavelengths were taken. 4. 50 µl of indicator was injected, manually mixed, and absorbance measurements at the acid, base and reference wavelengths were recorded.

Byrne determines the pK_a using Equation 6 as a function of salinity and temperature in seawater samples. The pH of a seawater sample is measured potentiometrically as absorbance measurements are taken (Robert-Baldo et al. 1985). Therefore, any uncertainties that may arise from using an electrode to measure pH will be passed on to the uncertainty of the pK_a . Consequently, spectrophotometric pH data cannot be considered any more accurate than potentiometric measurements. Byrne has made no claims that his method is truly accurate, however, it has been proven to be very precise and reproducible. Moreover, the activity term from the Henderson-Hasselbalch equation (Equation 5) is incorporated into the pK_a . Changes in solution activities are accounted for by the empirical relationship between salinity and pK_a . However, to adapt Byrne's method of seawater pH measurements to freshwater pH analysis, the pK_a of the indicator must be determined in low ionic strength solutions. Not only will freshwater pH spectrophotometric measurements suffer a similar pK_a uncertainty with respect to the pH of the buffer being determined potentiometrically, but the activity discrepancies between the dilute buffer and freshwater are unknown. This potential offset will be considered in the indicator characterization section.

Chapter 3

Methods

3-A.1 Characterization of the Indicator

Before the development efforts for the automated system began, we had to characterize the molar absorptivities and pK_a of an indicator. An indicator dye will be most effective if its pK_a is compatible with the expected pH range of local freshwater lakes and rivers (8.6 – 7.8 pH units for the Clark Fork River, L. Ronald unpublished data, 1999). If the pH range is within ± 1 of the pK_a , the signal / noise ratio will be optimized so that the whole range can be analyzed. Cresol red (CR), which has a reported pK_a near 7.8 (Byrne and Breland 1989), was chosen as the indicator dye for the automated system. In order to use CR it was necessary to determine the molar absorptivity ratios and pK_a .

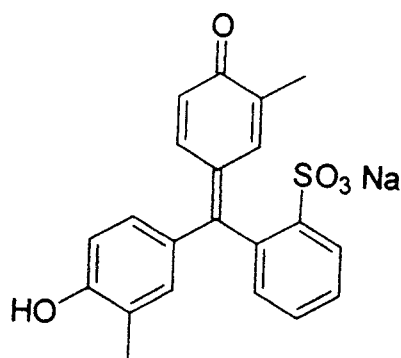


Figure 3-1. The molecular structure of cresol red.

Molar absorptivities were determined by obtaining absorbance spectra (as shown in Figure 2-1) of unpurified indicator solutions at approximate pH's of 12 and 4.5. These two pHs were chosen to ensure that CR would be exclusively in either the base or acid form. The molar absorptivity ratios in Equation 6 were determined at 439 and 577 nm for average absorbances over a range of ± 2 and ± 12 nm by applying Beer's Law

(Equation 4). The wavelength ranges selected as maxima correspond to the wavelengths and spectral band pass of the Lambda 11 UV-VIS spectrophotometer (Perkin Elmer) and spectrograph used in the lab study, respectively. Absorbance spectra were recorded at a constant temperature of 20.00 °C by using a 10 cm thermostated quartz cell (65-Q-100, Starna Cells, Inc). The ϵ_i are a very weak function of temperature (Zhang and Byrne 1995). Therefore, holding the temperature constant for ϵ_i measurements allows any ϵ_i temperature dependence to be incorporated into the pK_a , which is determined as a function of temperature. Figure 2-1 shows an example of the spectra used to determine the molar absorptivities and Table 3-1 and Table 3-2 summarize these results.

Table 3-1. Molar absorptivities at 20°C.

Molar absorptivity	12 nm bandwidth (L mol ⁻¹ cm ⁻¹)	2 nm bandwidth (L mol ⁻¹ cm ⁻¹)
ϵ_{a577}	48 ± 16	41 ± 16
ϵ_{a439}	23150 ± 10	23479 ± 6
ϵ_{b577}	2039 ± 21	2001 ± 39
ϵ_{b439}	61262 ± 76	66187 ± 131

Table 3-2. Molar absorptivity ratios at 20°C.

Molar absorptivity ratio	12 nm bandwidth	2 nm bandwidth
e_1	0.0021	0.0018
e_2	2.6463	2.8190
e_3	0.0881	0.0852

Once the e_i 's (as defined in Equation 7) were determined, it was possible to evaluate the pK_a by recording R values for a low ionic strength buffer solution (8.695×10^{-4} M KH_2PO_4 – 3.043×10^{-3} M Na_2HPO_4 , $\mu = 2.348 \times 10^{-2}$ M) (Covington 1983). Since the buffer solution's pH dependence on temperature was reported, this buffer was used to determine the temperature dependence of the pK_a . 40 μ L of 2.00 mM CR, which was made gravimetrically with filtered and degassed deionized water, was injected into the low ionic strength buffer. CR concentration in the 10 cm thermostated cell was approximately 5.7 μ M. The resulting R values obtained in the buffer solution were used to solve Equation 6 for pK_a . The results are shown in Figure 3-2. Variations of the pK_a with respect to temperature can be represented by equations of the form (Ramette et al. 1977):

$$pK_a = \frac{A}{T} + B + C \log T \quad (9)$$

where T is in Kelvin and A, B, and C represent thermodynamic constants. A, B, and C were determined by a nonlinear least squares analysis of the pK_a versus temperature, T. The results of this analysis produced:

$$pK_a = \frac{865}{T} + 2.092 + 1.300 \log T \quad (10)$$

Equation 10 not only provides an accurate fit for the pK_a data with respect to temperature, but its constants can be used to make estimates of thermodynamic properties such as standard changes in enthalpy (ΔH°), entropy (ΔS°), and heat capacity (ΔC_p°) of CR in the low ionic strength buffer (Ramette et al. 1977):

$$\Delta H^{\circ} = R(A \ln 10 - CT) \quad (11)$$

and

$$\Delta S^{\circ} = -R(B \ln 10 + C + C \ln T) \quad (12)$$

and

$$\Delta C_p^{\circ} = -RC \quad (13)$$

where T is in Kelvin and R is the gas constant ($R = 1.9872 \text{ cal K}^{-1} \text{ mol}^{-1}$).

Table 3-3. Calculated thermodynamic properties of CR in the low ionic strength buffer.

Temperature (K)	ΔH° (cal mol ⁻¹)	ΔS° (cal K ⁻¹ mol ⁻¹)	ΔC_p° (cal K ⁻¹ mol ⁻¹)
293.15	3201	-26.83	-2.583

The calculated ΔH° , ΔS° , and ΔC_p° for CR and phenol red (Robert-Baldo et al. 1985) show a similar magnitude.

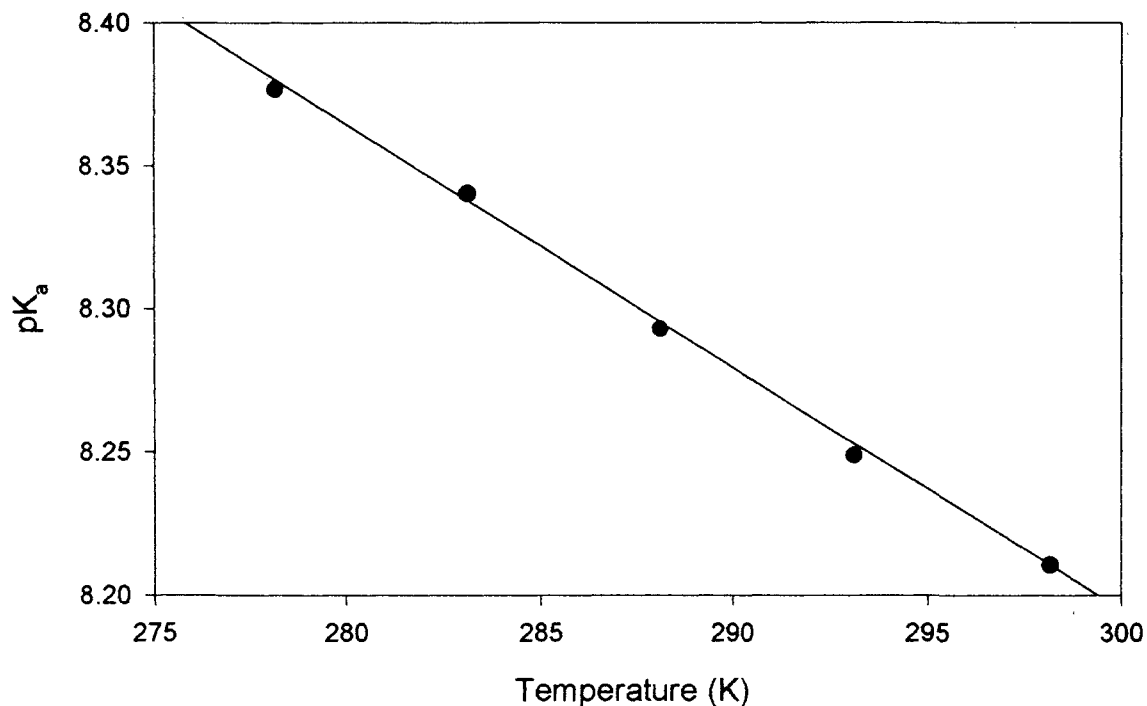


Figure 3-2. The pK_a of CR was determined with respect to temperature in buffers using a UV-VIS spectrophotometer and Equation 6. The regression line was produced from Equation 10, while the circles are the experimental data used to produce Equation 10. $r^2 = 0.999$.

3-A.2 pK_a Uncertainties

Fundamentally, our pH measurements are only as accurate to the “true” pH as our weakest link, the pK_a , will allow. Since the pK_a was determined with a low ionic strength buffer ($\mu = 0.02348$ M) that has a higher ionic strength than freshwater ($\mu < 0.005$ M), the activity coefficients (the γ term) in Equation 4 are significant. The extended Debye-Hückle equation could be used to solve for the γ term, unfortunately the hydrated radii of the ions are not known. If 800 and 600 pm were used as guesses for the HL^- and L^{2-} hydrated radii, the γ term would be -0.1844, which would indicate that our

effective pK_a is too small by 0.1844 when doing measurements spectrophotometrically (Harris 1982). However, since the uncertainty of this offset is quite high, we are reluctant to apply it. It is important to realize that if an alternative method to determine the pK_a more accurately is developed, we can easily apply it to previously recorded absorbance measurements. Since absorbance measurements are dependent on thermodynamic properties of the absorbing compound, good absorbance measurements are always valid. Not knowing the “true” pK_a however, does not prevent us from obtaining reproducible pH measurements, which will be discussed later in the results section.

3-A.3 pH Perturbation

In seawater measurements, the addition of indicator has been determined to perturb the sample pH slightly (≤ 0.005 pH units) because the indicator is a weak acid (Clayton and Byrne 1993). The pH perturbation is expected to be larger for freshwater because of its lower buffering capacity. Therefore, it is important to determine the theoretical effects of the indicator concentration on freshwater pH. A Quick Basic (Microsoft, Inc.) program, CRTURB.BAS (displayed in Appendix II), considers parameters such as the indicator, carbonate species, and water equilibria along with charge balance and mass balance equations to produce:

$$-[H^+]^2 + (\alpha_1 C_T + 2\alpha_2 C_T + \alpha_{2CR} [CR] - \text{Alk}) [H^+] + K_w = 0 \quad (14)$$

where [] denotes concentration, Alk is alkalinity, C_T is total inorganic carbon, K_w is the dissociation constant of water, and α is the ionization fraction and its subscript refers to the number of protons lost. Dilution effects of the sample by the indicator were factored

into the Alk and C_T . Dilution effects are minimal, $\approx 0.023\%$ indicator volume in the optical flow cell and does not significantly affect the pH. The α equations are:

$$\alpha_1 = \left(\frac{[H^+]}{K_1} + 1 + \frac{K_2}{[H^+]} \right)^{-1} \quad (15a)$$

$$\alpha_2 = \left(\frac{[H^+]}{K_1 K_2} + \frac{[H^+]}{K_2} + 1 \right)^{-1} \quad (15b)$$

$$\alpha_{1CR} = \left(\frac{[H^+]}{0.01} + 1 + \frac{K_a}{[H^+]} \right)^{-1} \quad (15c)$$

$$\alpha_{2CR} = \left(\frac{[H^+]}{0.01 K_a} + \frac{[H^+]}{K_a} + 1 \right)^{-1} \quad (15d)$$

The first dissociation constant of CR (assumed to be approximately 0.01) is much larger than the second (K_a). Therefore, at our expected pH range (7.8 – 8.5), $[H^+] / 0.01 \approx 0$. The program CRTURB.BAS iteratively solves Equation 14 for $[H^+]$. Alkalinity and total carbon were first determined using the program CO2SYS.EXE (Lewis and Wallace 1999) for a set pCO_2 (320 μ atm) and pH. The pH was varied (8.8 to 7.6 pH units) in order to produce varying Alk and C_T (i.e. varying buffer capacity). Figure 3-3 shows the theoretical pH perturbation caused by the addition of CR to samples with a wide range of alkalinities.

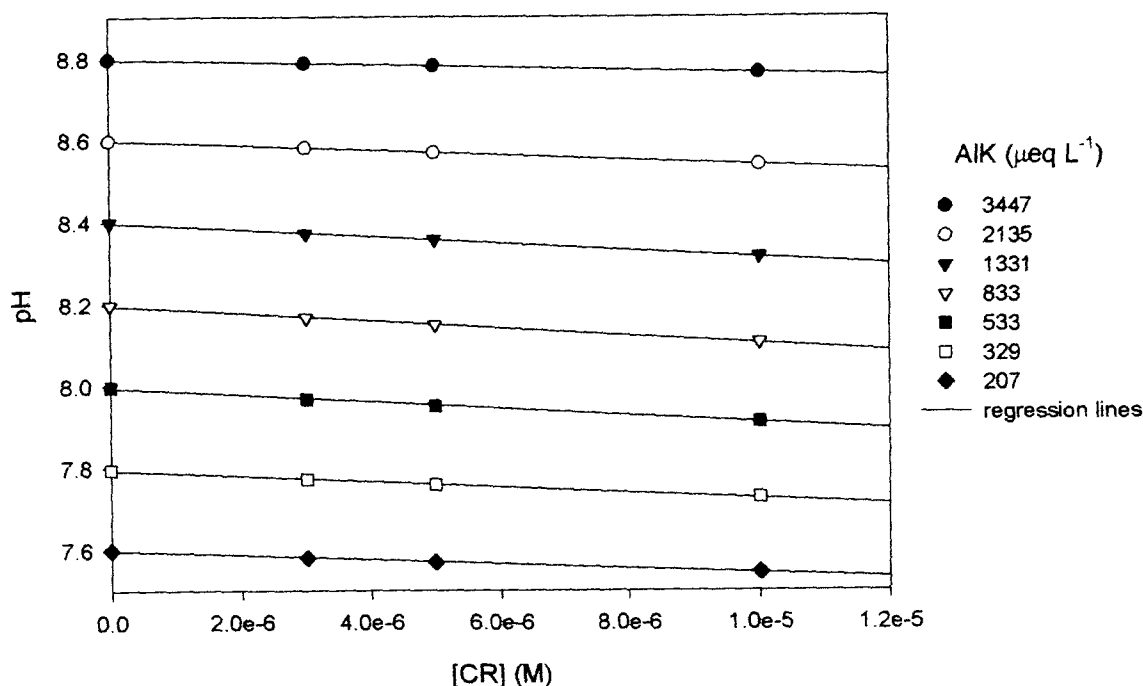


Figure 3-3. Theoretical pH perturbations caused by CR additions to samples with various alkalinities, $T = 20^{\circ}\text{C}$.

While looking at Figure 3-3, it is important to consider what concentration of CR is necessary for reasonable absorbance measurements. UV-VIS spectrophotometer measurements in a 10 cm cylindrical cell were taken with 3.0×10^{-6} M CR (0.4 – 1.0 absorbance units) while the autonomous lab pH instrument (2.0 cm optical pathlength cell) has reasonable absorbances (0.1 – 0.5 absorbance units) at approximately 5.0×10^{-6} M CR. The dependence of the pH perturbation on alkalinity is not readily apparent, however, a closer inspection of only the 5.0×10^{-6} M CR pH perturbations and slopes from Figure 3-3, shown in Figure 3-4, predicts that the indicator has less of an effect at higher and lower alkalinities. Higher alkalinities have greater buffering capacity and therefore, the pH is perturbed less. Water with less alkalinity has lower pH, closer to the pH of the indicator, and therefore its pH is perturbed less.

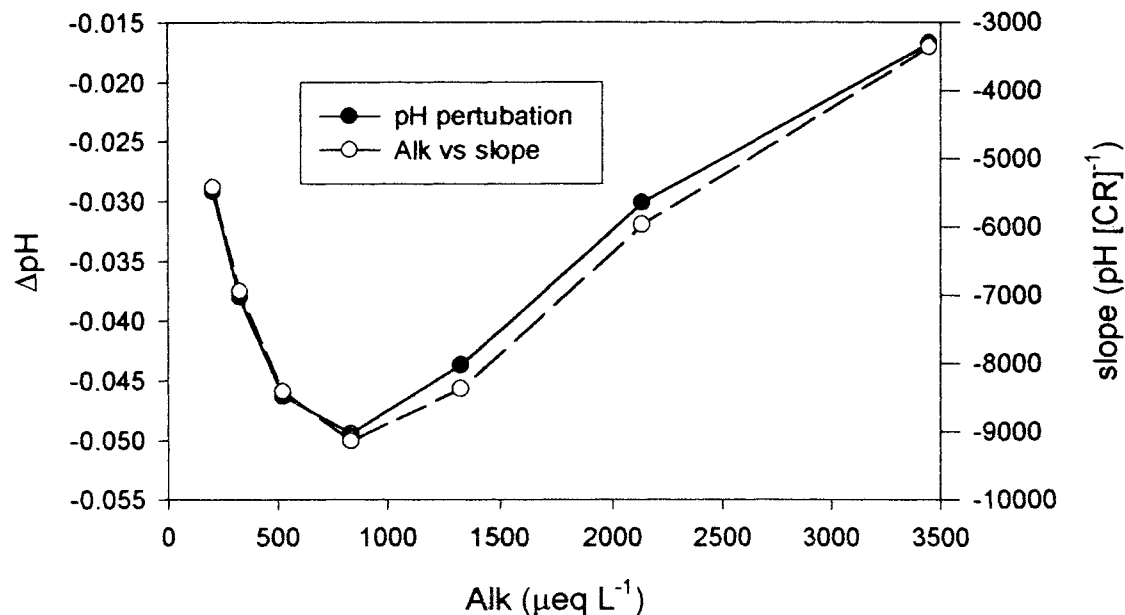


Figure 3-4. Theoretical pH perturbations (ΔpH), solid circles, of freshwater caused by 5.0×10^{-6} M CR for the alkalinities and pH listed in Figure 3-3. Negative ΔpH indicates that CR decreases the pH. The open circles are slopes versus alkalinities from Figure 3-3. $T = 20^\circ\text{C}$

A study of CR pH perturbations was conducted to evaluate our model. Absorbance measurements were recorded for additions of CR to freshwater in a thermostated 10 cm quartz cell using a UV-VIS spectrophotometer (Lambda 11, Perkin Elmer). Temperature was maintained at 20.00 ± 0.02 °C with a microprocessor-based waterbath (Neslab RTE-111) by circulating water through the jacketed cell. After each addition of 8.0 μL 1.88 mM CR, absorbance measurements were recorded. Alkalinity, which was determined by the Gran titration method (performed by J. Reynolds), and the $p\text{CO}_2$, which was set at 320 μatm by bubbling with 360 ppm CO_2 gas for 15 minutes, were entered into CO2SYS.EXE to solve for pH and C_T . The theoretical plot was then produced in CRTURB.BAS by varying the [CR] while holding Alk, C_T , and temperature

constant as in Figure 3-2. As can be seen in Figure 3-4, the theoretical and experimental pH perturbation do not agree.

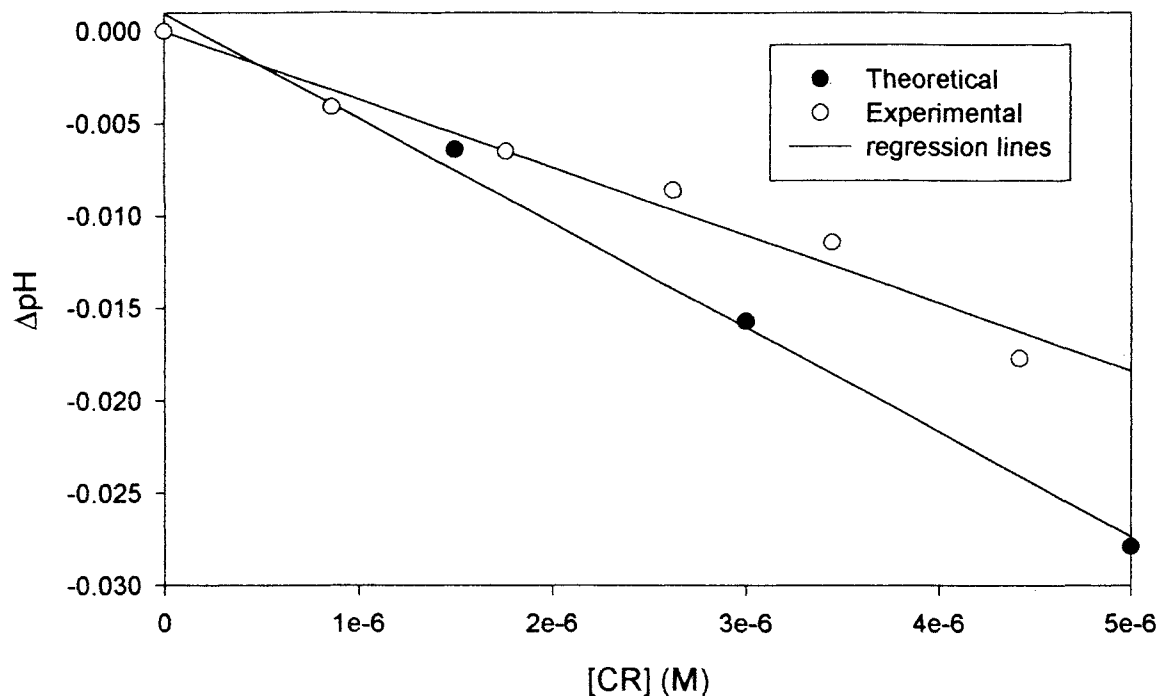


Figure 3-5. Comparison of theoretical ($\Delta\text{pH} = 9.388 \times 10^{-4} - 5658[\text{CR}]$, $r^2 = 0.994$) and experimental ($\Delta\text{pH} = -1.691 \times 10^{-5} - 3673[\text{CR}]$, $r^2 = 0.95$) CR pH perturbation. $\text{Alk} = 2045 \mu\text{eq L}^{-1}$, $C_T = 2035 \mu\text{mol L}^{-1}$, and $T = 20.00^\circ\text{C}$ were applied for the theoretical line. $[\text{CR}]$ is the total CR concentration. $\Delta\text{pH} = \text{pH}_{[\text{CR}]} - \text{pH}_0$, the pH at $[\text{CR}] = 0$, pH_0 , was found by extrapolation.

3.A.4 CR Purification

The difference between the theoretical and experimental results illustrated in Figure 3-5 motivated us to investigate the nature of the CR indicator further. Since the CR did not perturb the pH as much as we predicted, we suspect that its pH must be higher than we assumed. To test this, both a purified CR solution and a 95% pure sodium salt CR solution were diluted to $5.08 \times 10^{-4} \text{ M}$ and $4.76 \times 10^{-4} \text{ M}$ CR, respectively. Dilutions

were necessary to reduce the magnitude of the absorbance. Table 3-4 contains the measured pH, determined in a 1.0 mm cuvet using the UV-VIS spectrophotometer, and the theoretical pH for both CR solutions (calculated using Equation 14 with $C_T = 0$ and $\text{Alk} = 0$). Previously we had assumed that the CR pH was approximately 5.0

Purification of 95% pure CR (not from sodium salt) was attempted by recrystallization from glacial acetic acid. The purification was evaluated by observing the change of the molar absorptivity of the L^{2-} form. An increase in the molar absorptivity of 3.7% was observed. Since CR in the protonated form is not very soluble in water, a NaOH solution was used to dissolve the purified CR. The purified indicator solution was 2.02 mM NaOH and 2.064 mM CR. This is the "purified" entry in Table 3-3.

Table 3-4. Spectrophotometric pH measurements of diluted CR solutions.

CR solution	[CR] (M)	pH
Purified (not from Na salt)	5.08×10^{-4}	6.90 (experimental)
95% pure (from Na salt)	4.76×10^{-4}	7.64 (experimental)
Theoretical 100% pure CR (from Na salt)	5.00×10^{-4}	5.79 (theoretical)

Table 3-4 indicates that the 95% pure CR (from Na salt), as compared to the theoretical 100% pure CR, has an unknown source of alkalinity raising its pH above 7. We will be able to estimate the alkaline equivalence of the impurities by the theoretical calculations. Increasing alkalinity to $9.52 \times 10^{-5} \mu\text{eq L}^{-1}$, which would require impurities up to 20% of 4.76×10^{-4} M CR, theoretically increases the pH to 7.65 pH units. Further investigations, however, are required before any theoretical pH perturbation correction

can be implemented. To briefly summarize, the expected pH perturbation due to addition of CR is ~ 0.03 pH units (Figure 3-5) for an alkalinity typical of the Clark Fork River. Further purifications of the indicator should improve the comparison between the predicted and experimental data.

3-B Instrumentation Design

3-B.1 Instrumental Layout

All experiments to date have been executed with a laboratory version of the planned in situ pH instrument. Figure 3-6 is a schematic diagram of the autonomous laboratory pH instrument, called ALpHI for short. ALpHI is designed to deliver small amounts of CR into a pulsating sample stream so that the absorbance of the CR / sample solution can be measured.

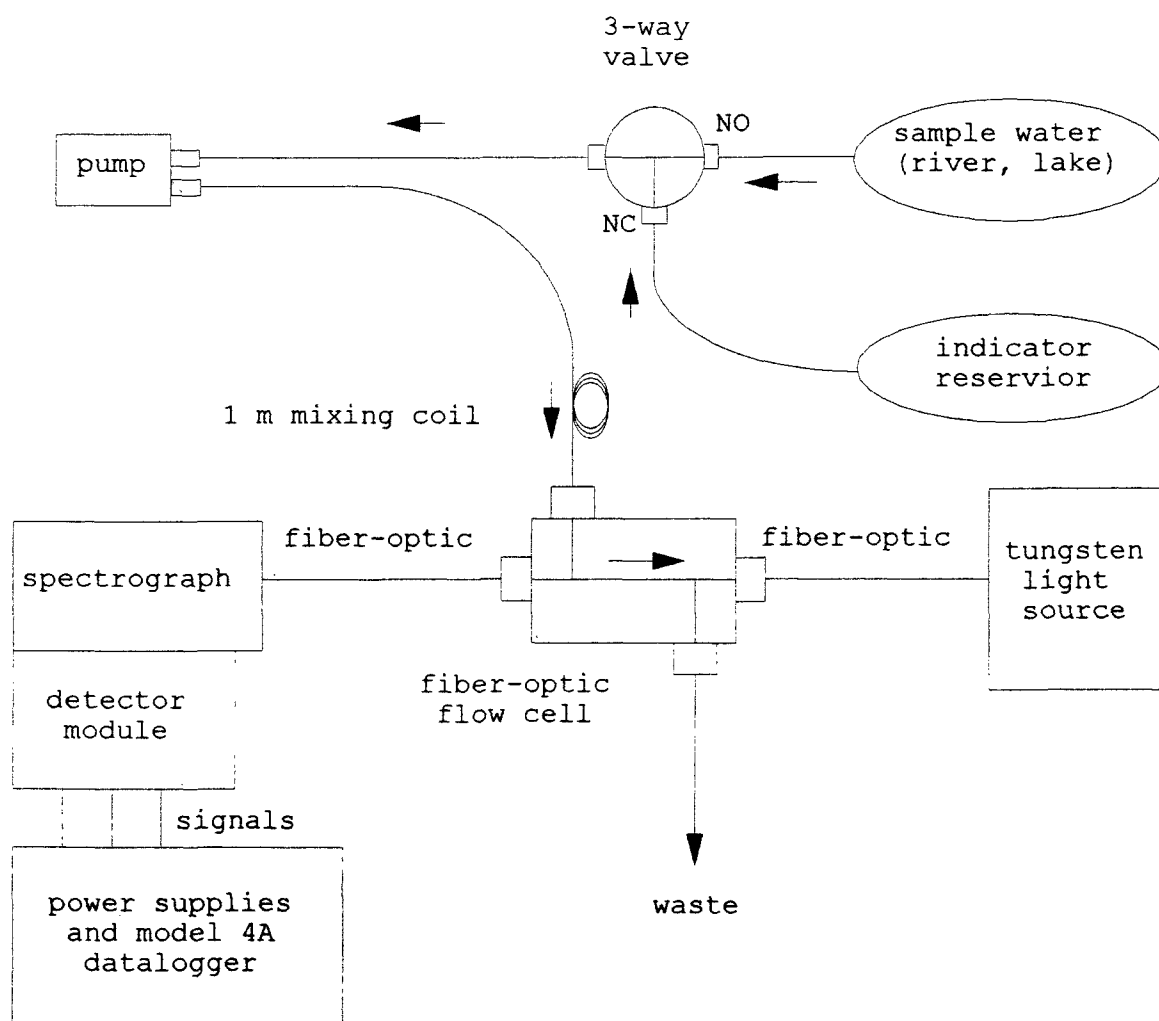


Figure 3-6. ALpHI layout (NC = normally closed, NO = normally open).

The plumbing portion of ALpHI (Figure 3-6) consists of a solenoid pump (LPLA1210050L, The Lee Co.), that pulls either from an indicator reservoir or directly from the freshwater sample at a rate of $50 \mu\text{L min}^{-1}$ (1 pulse per minute). A three-way solenoid valve (LFYA1218032H, The Lee Co.) opens briefly permitting indicator to flow into the sample stream. Changing the time the valve is engaged can therefore vary the concentration of indicator. The indicator pulse travels through a 1 m mixing coil (PEEK 1.0 mm ID). A long and large ID mixing tube allows frequent, small CR pulses to disperse more uniformly before reaching the flow cell. Therefore, the concentration of CR in the flow cell will vary less, which in turn allows for measurements that are more consistent. Any air bubbles within the flow cell obstruct the optical pathway (Figure 3-7). A smaller inner diameter tube (PEEK 0.18 mm ID) is attached at the flow cell outlet to supply backpressure, which prevents bubbles from permanently lodging in the cell. Because of the backpressure, the $50 \mu\text{L}$ pump pulse requires 25 minutes until the pulse reaches the flow cell from the valve. Power requirements are minimized because the pumps and valve are on for less than two seconds per pulse. All on-off switches are controlled by a low power, compact data logger (TattleTale 4A, Onset Computer Corp.).

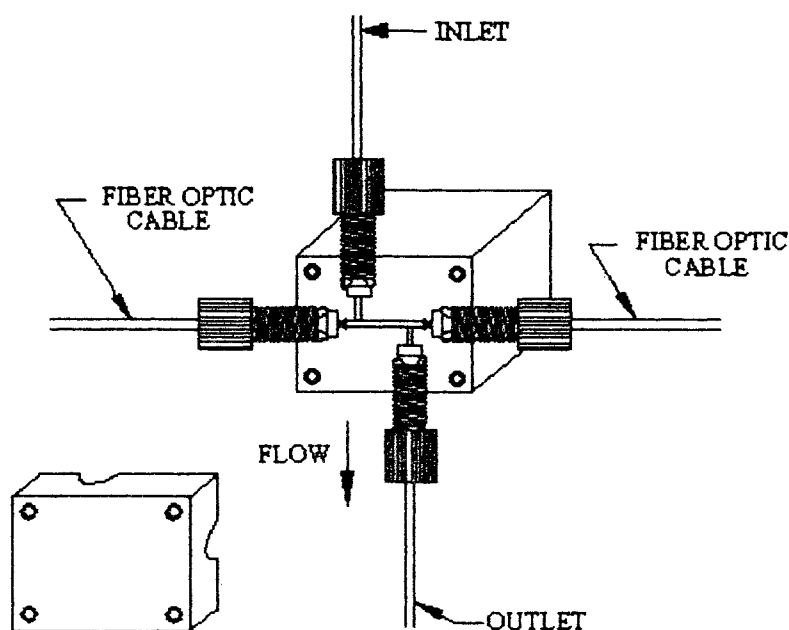


Figure 3-7. A cut away view of the flow cell (made from high density polyethylene), where INLET is from the mixing coil, OUTLET is the backpressure coil, and the FIBER OPTIC CABLE comes from the light source and goes to the detector (adapted from DeGrandpre et al. 1995)

The optical components of the lab pH instrument (shown in Figure 3-6) consist of a tungsten lamp (5 V, 0.12 A, Gilway Technical Lamps), two sections of 400 μm core fiber-optics (HCN-M0400T, SpecTran Specialty Optics Co.), a 0.5-mm-ID flow cell (Figure 3-7), a small spectrograph (MS10, American Holographic, Inc.), and three photodiode detectors (G1962 and S2386-5K, Hamamatsu Corp). Light travels to the flow cell via one fiber where it is attenuated across the optical pathlength before being transmitted via the other fiber to the spectrograph. Initially the cell pathlength was 0.75 cm, however, to decrease the concentration of CR, we later obtained a 2.0 cm flow cell. Because we changed the flow cell, the 400 μm core fiber-optics were replaced with 600

μm core fiber-optics (F-MSC-OPT, Newport Corporation) to increase light throughput. The fibers are secured at both ends of the cell by o-rings and plastic fittings (1/16" P•200, Upchurch Scientific). The three photodiodes are centered at the following wavelengths: 439, 577, and 724 nm with spectral bandpasses of ± 12 nm. Using a GaP photodiode (G1962, Hamamatsu) that is insensitive to near infrared (NIR) radiation eliminates the effects of stray light at the 439 nm channel (DeGrandpre et al. 1999). Data from 0 – 5 volts are stored in the data logger as digital voltage from 0 to 4095 corresponding to the data logger 12-bit analog-to-digital converter

Each measurement cycle, which was controlled by an operating program (ALPHI1.TT4, displayed in Appendix III), consists of the following sequence: 1. Time (t) = 0 - 0.1 s: the valve is engaged, 2a. t = 0.1 - 0.11 s: while using the Lee Co. valve, the valve is switched off and then the pump is engaged, allowing a slug of indicator to be pulled into the pump, 2b. t = 0.1 - 0.11 s: while using the Neptune valve, the pump is engaged and the valve is switched off after 0.01 s, allowing a slug of indicator to be pulled into the pump, 3. t = 2 sec.: the pump solenoid is deactivated, 4. t = 2 s - 4 min.: three pulses of sample water are pumped, 5. t = 4 min.: the detector is turned on and allowed to warm up for 20 s during another sample pulse, 6. t = 5 min.: detector dark signals are recorded, the lamp is turned on, and another sample pulse occurs, 7. t = 5.5 min.: each detector channel averages 65 readings over 2-s intervals to produce 8 averaged signals for each I_λ and temperature, 8. t = 6 min.: the lamp and detector are turned off, and the system is ready for the next cycle to begin. Because one pulse takes 25 minutes to reach the optical flow cell from the valve, each cycle measures the pH of the sample that entered the valve 25 minutes ago.

Figure 3-8 is an example of one indicator pulse traveling through the system. The cycle described above is designed to maintain a constant indicator concentration and therefore does not produce data like Figure 3-8. The pulse, however, illustrates a few of the important concerns, such as the minimum and maximum indicator concentrations and pH perturbation. Signals were measured every 2 s beginning just prior to the indicator slug reaching the flow cell. Viewing the pH and indicator concentration together allows us to evaluate their relationship. $[CR]$, which is the total indicator concentration, was calculated through Beer's Law and the $(R - e_1) / (e_2 - Re_3)$ term of Equation 6. Once the concentration increased to more than 3×10^{-6} M CR the signal to noise ratio improved dramatically, even though the absorbances at this concentration (0.031 absorbance units and 0.056 au for the 439nm and 577 nm channels, respectively) are very low. At peak $[CR]$, 1.42×10^{-5} M, the absorbances are more reasonable, 0.158 au and 0.254 au for the 439 nm and 577 nm channels, respectively. Therefore, we are able to use relatively low absorbances to produce stable pH calculations, which is advantageous because at high $[CR]$ the pH perturbation is larger (Figure 3-5).

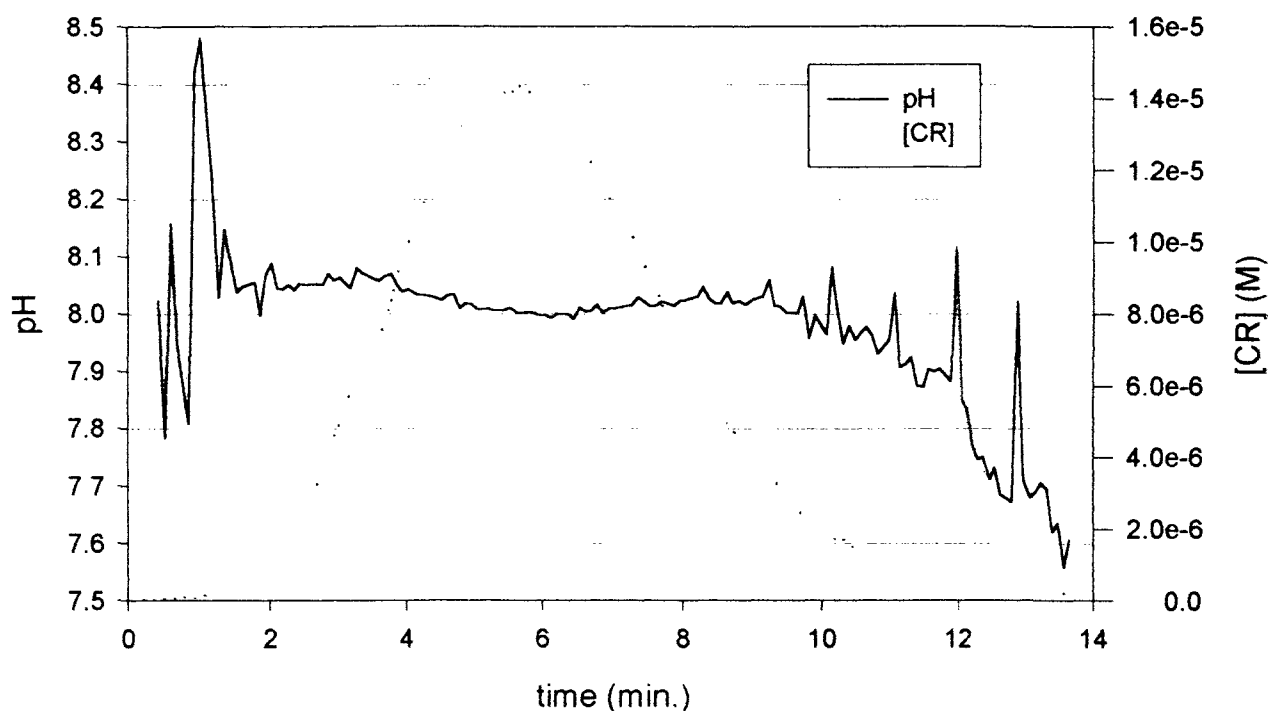


Figure 3-8. An example of constant measurements as one pulse travels through the 0.75 cm flow cell. The Neptune Research valve was used.

The pH 'dip' in Figure 3-8 signifies that we must find a balance between adequate absorbance and the pH perturbation that it will cause. Initially the data was culled over to find the timing for the best balance of a single pulse. Then the system was adjusted to collect data only during this window; however, this practice was not very effective. Variances in the size of the indicator pulse continuously made the measurements irreproducible. Finally, we concluded that a constant sample / CR ratio would produce the best results. In order to maintain this ratio, a larger mixing tube (1 m, 0.10 cm ID, total mixing tube volume = 0.79 mL) was installed and smaller, more frequent CR pulses were passed through the valve. Timing of the cycle described previously is designed to

control the sample / CR ratio which provides a more reproducible indicator concentration and hence, pH. A typical measurement cycle is displayed in Figure 3-9.

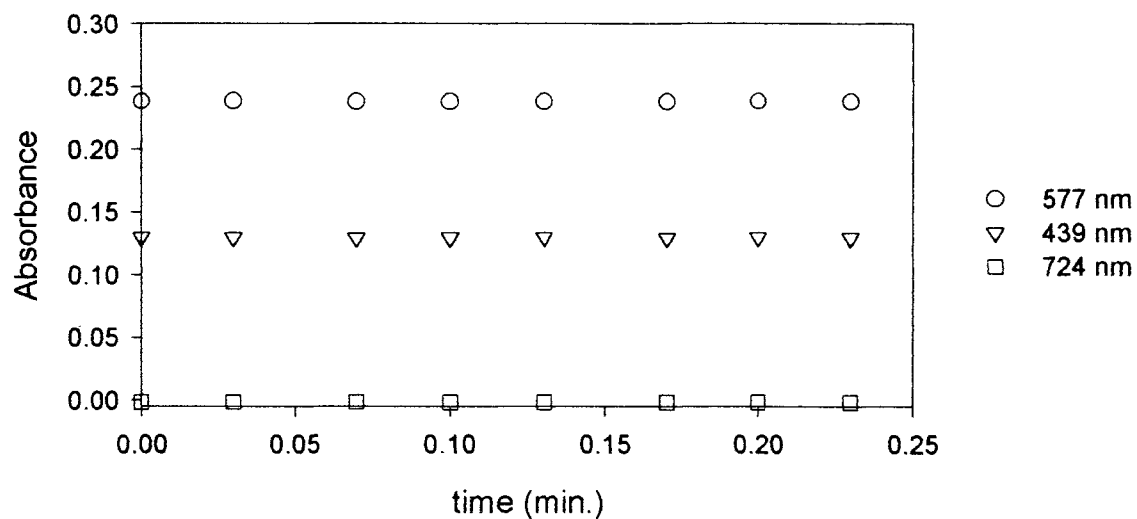


Figure 3-9. An example of one measurement cycle for a freshwater sample.

3-B.2 Blank Measurements

Equation 8, which calculates the absorbance from the digital voltage signals, was enhanced by adding the term K_λ to form Equation 16:

$$A_\lambda = -\log\left(\frac{I_\lambda}{K_\lambda I_{\text{ref}}}\right) \quad (16)$$

where A_λ is the indicator absorbance, I_λ is the transmitted light intensity at an absorbing wavelength (439 or 577 nm), I_{ref} is the transmitted light intensity at a nonabsorbing wavelength (724 nm), and K_λ is $I_o / I_{o\text{ref}}$ where I_o is the transmitted intensity of the blank at λ and $I_{o\text{ref}}$ is the transmitted intensity of the blank at 724 nm. The blank constant K_λ corrects for fluctuations in the transmitted intensity between blanks, which allows blanks

to be run less frequently (DeGrandpre et al. 1995). New K_{λ} values are calculated each time a blank is run.

Quality blank values (K_{λ}) were difficult to obtain in the early days of this research because there always seemed to be a trace of indicator in the flow cell. Since dead volume in the valve was the likely source of indicator, it became necessary to manually bypass the valve from the plumbing system so that K_{λ} values could be determined. The cell was flushed without the backpressure tube to allow for higher flow rates for 7.5 minutes (at a rate of 20 pulses per minute) with sample water. The backpressure tube was reattached and the K_{λ} values were recorded after one hour of stable signals (no air bubbles). Although this tedious method is effective for the laboratory version, it is impractical for in situ deployments. By replacing the Lee valve with a Neptune Research valve (E-01367-72, Cole-Parmer), the need to bypass the valve was eliminated. Figure 3-10 demonstrates the much more rapid flushing that is possible with the Neptune Research valve compared to The Lee Co. valve.

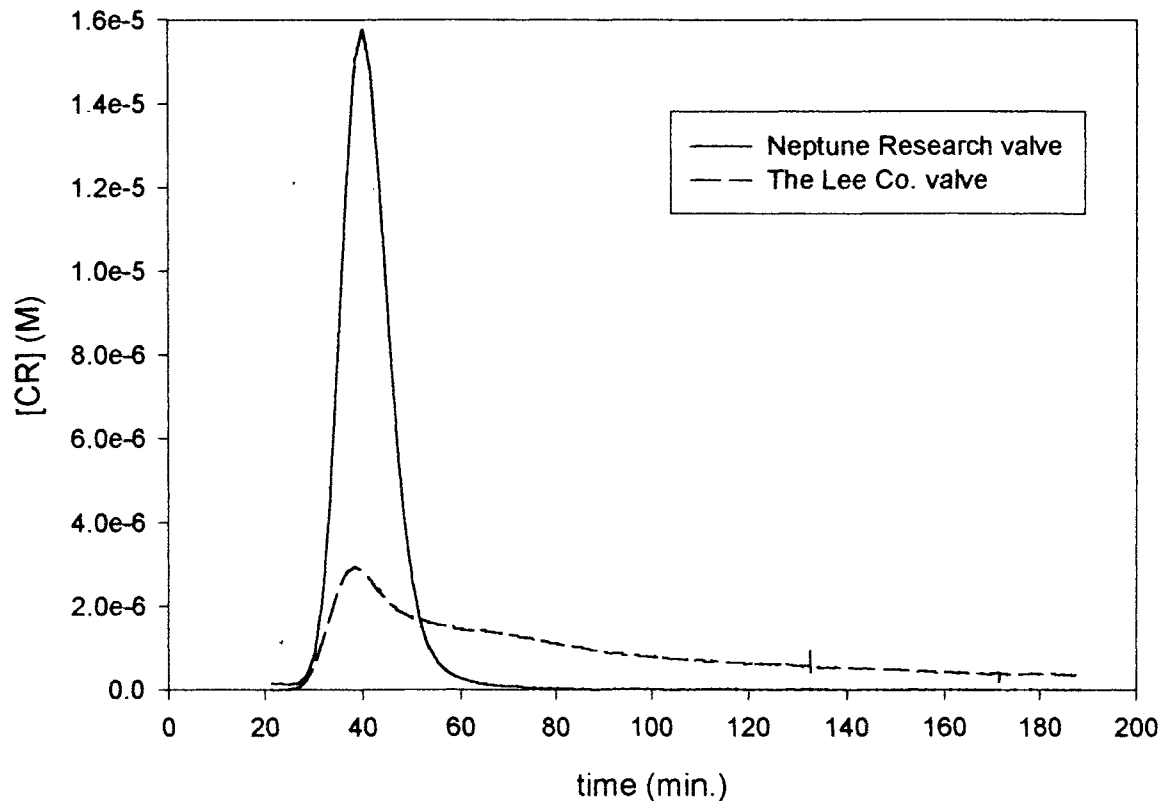


Figure 3-10. The Lee valve is not clear after the duration of the test, while the Neptune Research valve is clear of CR within 80 minutes. The pump rate was 1 pulse (50 μ L) of freshwater per minute for both valves.

The superior indicator flushing with the Neptune Research valve can be explained by comparing the designs of the valves. Instead of the pinch style of The Lee Co. valve, the Neptune Research valve engages a piston with different channels. The channels are separated vertically and lead to either normally open, NO, or normally closed, NC. Consequently, The Lee Co. valve allows residual indicator to remain in contact with sample line, while the Neptune Research valve literally walls off the flow of indicator.

3-B.3 Evaluation of the Plumbing System

Response time of ALpHI is the time required to detect 90% of a pH change following a change of sample solutions. Figure 3-11 shows an example of pH measurements following such a change. The change takes place at time = 0 minutes and measurements are recorded at 12.57 minute intervals. The flow rate is $50 \mu\text{L min}^{-1}$. pH averages and 3σ precision for each measurement cycle ($n = 8$) indicate that the response time is approximately 50 minutes.

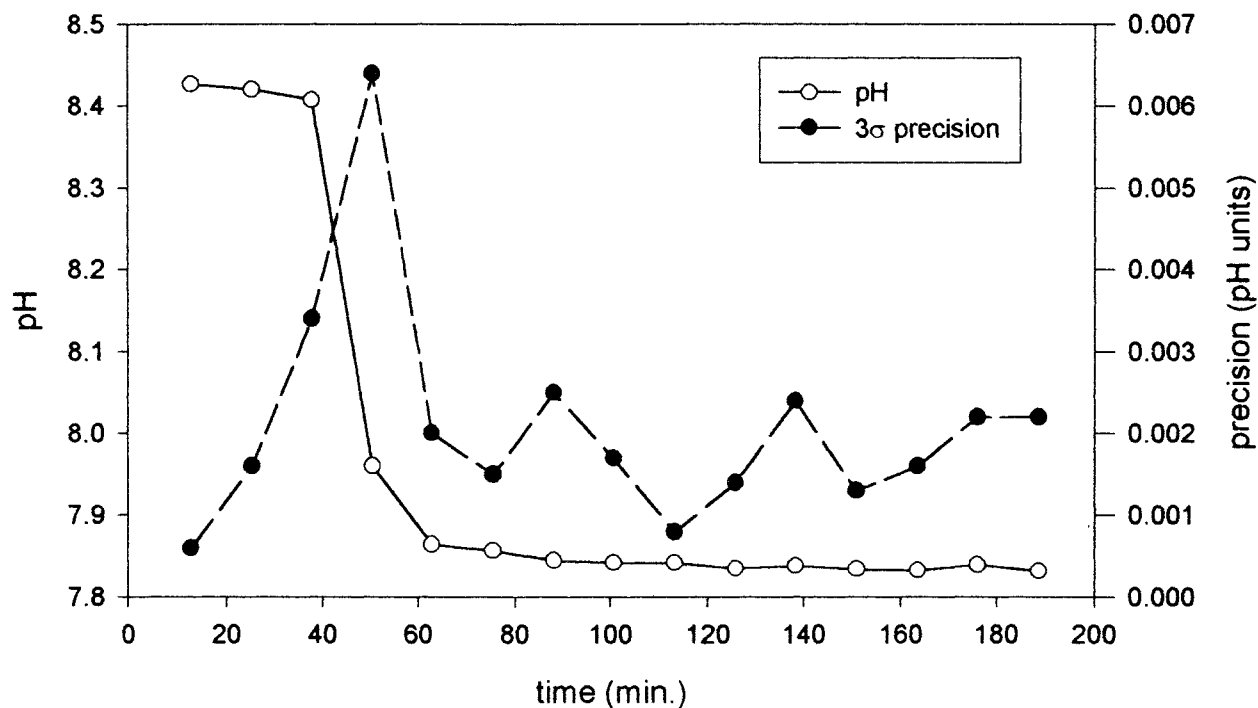


Figure 3-11. A study of the response time required to change freshwater samples, sample changed at $t = 0$.

3.B.4 Evaluation of the Optical System

Wavelength calibration

Before the instrument was used to measure pH, the spectrograph had to be calibrated to the correct wavelengths. The wavelengths of maximum absorbance for the acid and base forms of CR are 433 nm and 573 nm, respectively, and the reference channel is at 724 nm. However, because of the commercial availability of inexpensive 577 nm bandpass filters, we calibrated the base channel to 577 nm. A 577 nm bandpass filter (577FS05-25, Andover Corporation) was placed between the light source and the fiber-optic, and the grating was adjusted until the signal intensity was maximized. The other two photodiodes, mounted at appropriate distances from the center photodiode according to the linear dispersion of the grating (9.5 nm mm^{-1}), are therefore, calibrated simultaneously. The location of the acid channel photodiode is $\sim 439 \text{ nm}$.

Optimizing the signal

Care was taken to optimize light throughput by monitoring the reference channel. Fiber-optic ends were checked for flaws and cleaned regularly. The fiber-optic facing the light source was then adjusted three dimensionally while a multimeter monitored the signal. Once the light throughput was maximized, the fiber-optic cable was secured in place and new blank values were promptly measured.

Stray light

Stray light, i.e. light that is not within the specified bandpass at the 439 nm and 577 nm channels, was determined by first measuring the light and dark detector signals

using a multimeter. A 700 nm long pass filter (700FH90-25, Andover Corporation Optical Filters) was then placed in front of the light source, and the filtered signals were measured. The dark signals were subtracted from the light and filter signals before the percent stray light was determined. Stray light at the 439 nm and 577 nm channels was typically 0.16% and 0.28%, respectively.

3-C Relative Accuracy Experiments

It was necessary to have a reference method for comparisons to the ALpHI measurements. Relative accuracy experiments were designed to evaluate ALpHI pH measurements (pH_A) with respect to UV-VIS spectrophotometer pH measurements (pH_U). Three experiments, in which the error was reported as $\text{pH}_A - \text{pH}_U$, were used to quantify the relative accuracy. Initially relative accuracy experiments were conducted with buffer solutions because the indicator would cause only a minor pH perturbation in such solutions. Therefore, the buffer solution relative accuracy experiments represent the best possible relative accuracy we could expect. The second set of relative accuracy experiments were performed with freshwater, however, the results were not encouraging due to large pH perturbations. We switched flow cells from the 0.75 cm to the 2.0 cm for the final freshwater relative accuracy experiments. The longer pathlength flow cell allowed us to decrease [CR], while still maintaining reasonable absorbances. Methods used in these experiments are described in the following sections, while the results are listed and discussed in the next chapter.

3-C.1 Buffer Solution Preparation

Two buffer solutions were used for the relative accuracy experiment. Buffer solutions in the range 7.2 to 8.0 pH units were made with KH_2PO_4 , while the buffer solutions for the higher range (8.3 to 8.8 pH units) were made with H_3BO_3 . Stock solutions (0.100 M) for both buffers were prepared by dissolving the appropriate quantity in 1.00 L of degassed DI water. The buffer solution recipes were prepared by diluting

50.0 mL of the stock solution plus x mL 0.100 M NaOH to 100 mL with degassed DI water (Bower and Bates 1955).

3-C.2 Freshwater Sample Preparation

Water samples were collected as needed from the Clark Fork River in Missoula, MT for the freshwater relative accuracy experiments. The Clark Fork River was chosen as our source of freshwater because it is a likely candidate for a future in situ deployment. Freshwater samples were promptly sterilized by adding $100 \mu\text{L L}^{-1}$ saturated HgCl_2 and filtered to remove particulates. In order to evaluate ALpHI at various pH, small additions of 0.974 N HCl were made to the freshwater samples. The concentration of aqueous CO_2 was held constant for all freshwater samples by bubbling each sample with 360 ppm CO_2 gas at 20.0°C ($\pm 0.2^\circ\text{C}$) in a constant temperature water bath (Model 1166, VWR Scientific) for 15 min.

3-C.3 ALpHI Procedure

The ensuing procedure was followed for all samples used for the relative accuracy experiments: (1) the sample preparation for either buffer or freshwater was completed as described previously; (2) all possible air was removed from the sample reservoir (a sample bag) with a syringe; (3) the sample reservoir was filled with the new sample; (4) the sample reservoir was elevated as it was reattached to the valve so that air bubbles would not enter the system; (5a) if The Lee Co. valve was being used, the valve was manually bypassed; (5b) or, if the Neptune Research valve was on line, it was simply not engaged; (6) K_λ and I_{oref} values were obtained as described in section 3.B.1 for Equation

16; (7) the valve was restored to functional status and the first measurement cycle was initiated. Data were not recorded, however, until the reference signal stabilized, indicating that the system was void of air bubbles.

3-C.4 UV-VIS Spectrophotometric pH Measurement Procedure

All pH_U measurements were made with a UV-VIS spectrophotometer before and after ALpHI measurements to check the relative accuracy of the ALpHI for each sample. A syringe was used to fill the 10 cm thermostated quartz cell. The cell was placed in the measurement compartment, constant temperature was maintained (± 0.02 °C) with a microprocessor-based water bath (Neslab RTE-111), and the sample was analyzed by the UV-VIS spectrophotometer after initiating the ALpHI. After the ALpHI measurements were completed, the remaining sample from the reservoir was poured into the 10 cm thermostated quartz cell for a second pH_U measurement. A 2.010 mM CR solution was used as the indicator stock solution.

The spectrophotometric measurements were made in the following manner: (1) the 10 cm cell was filled with approximately 13 mL of sample and connected to the constant temperature water bath by tubing; (2) after temperature equilibration at the anticipated ALpHI temperature, a multiwavelength blank was recorded for 439, 577, and 724 nm; (3) 25 μL of the indicator was injected into the cell by using a 100 μL micropipet; (4) the cell was removed and the contents mixed; (5) absorbances at 439, 577 and 724 nm were then recorded. The pH was calculated from Equation 6 using the measured absorbances, temperature of the water bath, and the 2.0 nm bandwidth ϵ_i 's from Table 3-2.

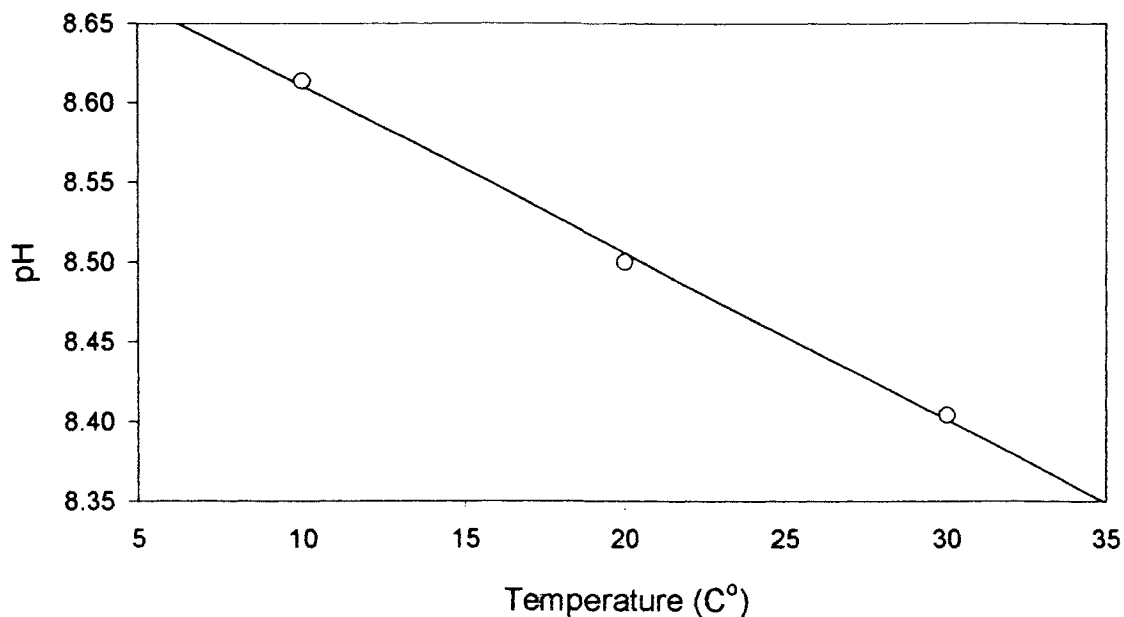


Figure 3-12. Theoretical pH changes with temperature for a freshwater solution with $\text{Alk} = 1684 \mu\text{eq L}^{-1}$ and $C_T = 1673 \mu\text{M}$. $\text{pH} = 8.7153 - 0.011T$, $r^2 = 0.998$.

3-C.5 Freshwater Temperature Compensation

More often than not, the ALpHI and UV-VIS spectrophotometer temperatures for a given sample were not the same. The temperature of the pH_L measurement was set at an anticipated pH_A measurement temperature. However, because it would be difficult to thermostat the entire ALpHI, its sample temperature fluctuates with the room temperature. The freshwater pH_A measurements were adjusted to agree with the temperature of the pH_U measurements by applying a theoretical slope of $-0.011 \text{ pH units C}^{-1}$ (from Figure 3-12), which was determined using a Quick Basic program, CO2SYS.BAS (Lewis and Wallace 1999). Since temperature affects are a weak function of alkalinity, we were able to use only one theoretical Alk. Theoretical Alk and DIC were set at $1684 \mu\text{eq L}^{-1}$ and $1673 \mu\text{M}$, respectively, so that the pH at 20.0°C would be

8.5 pH units. Temperature adjusted pH_A measurements are used to determine the reproducibility of the ALpHI.

Chapter 4

Results

4.1 Buffer Solution Relative Accuracy Experiment

The relative accuracy of ALpHI was evaluated using buffer solutions and a 0.75 cm pathlength fiber-optic flow cell. Graphs of absorbance, temperature, and pH versus time were produced for each sample. Examples of these results are shown in Figures 4-1 and 4-2. Note that the reference channel remains near zero (± 0.001 au) while the two analytical wavelengths vary due to their dependence on solution pH and indicator concentration. Therefore, in the subsequent absorbance graphs the reference channel will be omitted. Graph 4-1A displays a typical absorbance range. Absorbance and temperature data from Figure 4-1 were used to calculate pH with Equation 6. The pH data for buffer sample 100798a is shown in Figure 4-1C and 4-2 with 3σ error bars. Typical 3σ levels for the buffer solutions were $\pm 0.001 - 0.003$ pH units.

CR concentrations were calculated as described in section 3.B.1 and plotted with pH in Figure 4-2. Typically, the buffer solution pH displayed a weak correlation with respect to [CR]. However, as the temperature increases, the pH decreases. Buffer solution pH appears to be more dependent on temperature fluctuations ($r^2 = 0.83$) than on [CR] ($r^2 = 0.51$). Therefore, the concentration of indicator in the buffer solutions is of little concern as long as we are able to acquire reasonable absorbances.

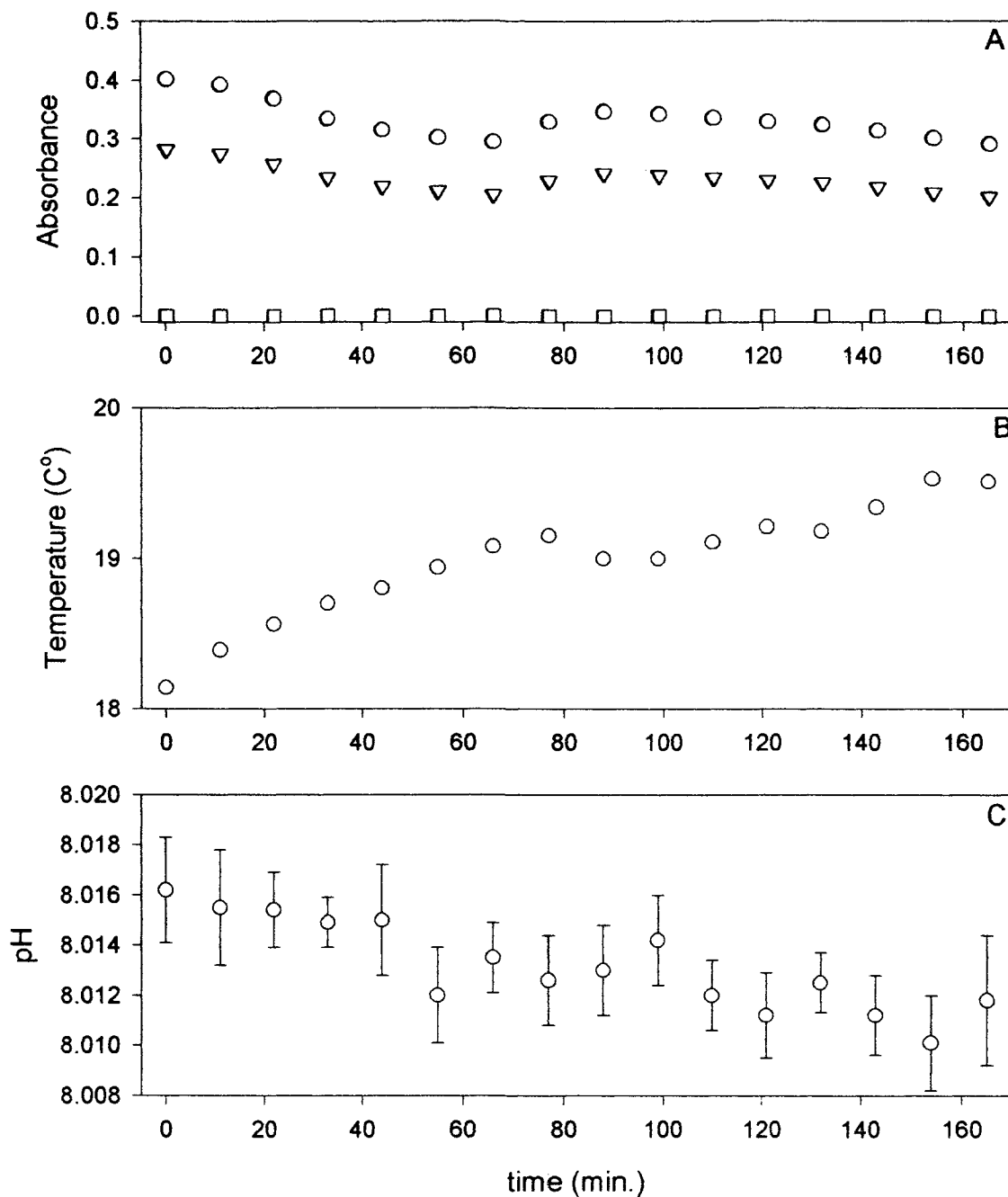


Figure 4-1. Data recorded from a sample of boric acid buffer solution (sample 100798a). A. Clusters of absorbance measurements, ○ = 577 nm, ▽ = 439 nm, and □ = 724 nm, are overlying data points from each measurement cycle (one measurement cycle is displayed in Figure 3-9). B. Temperature measurements. C. ALpHI pH measurements with 3σ error bars.

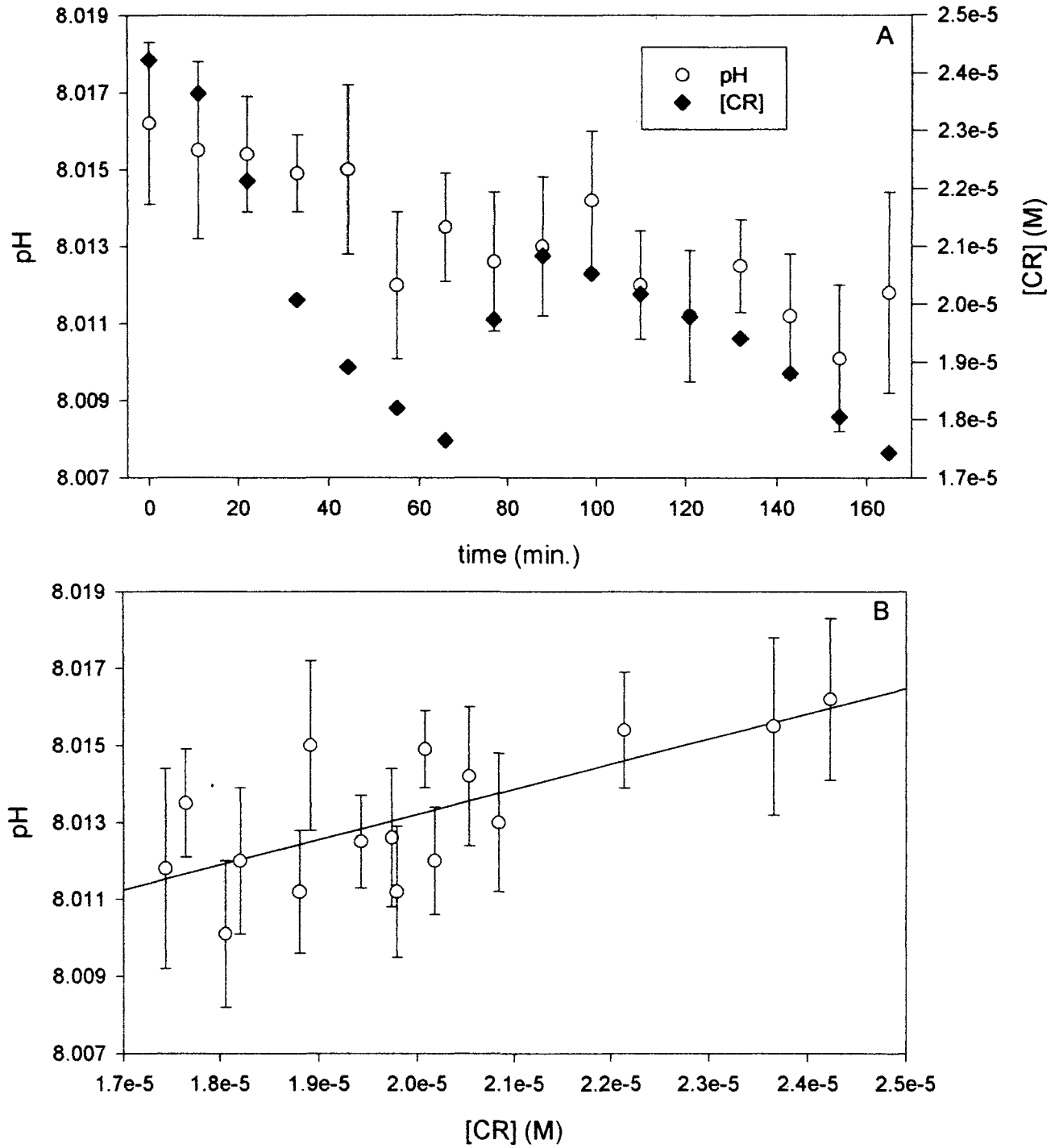


Figure 4-2. Graphs A and B were used to determine the correlation between pH and [CR], the regression line in graph B is $\text{pH} = 8.0001 + 654.4[\text{CR}]$, $r^2 = 0.51$. $\text{pH}_U = 8.018$.

Eight buffer solutions, including 100798a (Figure 4-2), with pH varying from 7.2 – 8.8 pH units were analyzed. The relative accuracy of the ALpHI was determined by comparing to the UV-VIS spectrophotometer for each sample. Figure 4-3A compares the correlation of these results to a 1:1 correlation line, while Figure 4-3B shows the error between pH_A and pH_U for each sample. Each circle in Figure 4-3A represents an average pH_A ($n = 8$) for one sample. Error bars in Figure 4-3B represent the 3σ of the average pH_A for each sample.

Using the buffered solutions allowed the performance of ALpHI to be evaluated while limiting the pH perturbation caused by the addition of CR. The series of buffer solutions ranging in pH from 7.2 to 8.8 pH units provided insights into the working range of ALpHI. ALpHI's working range of pH should be limited by the CR pK_a because as the pH increases or decreases CR equilibria will adjust accordingly. Therefore, if pH increases, CR will eventually be exclusively in the base form and the acid channel absorbance will be mostly noise. The relative accuracy within the range 7.6 to 8.6 pH units was ≤ 0.01 pH units, but increased to > 0.03 pH units once outside of this range, as can be seen in Figure 4-3B. Direction of the pH perturbation is controlled by the relationship between the sample and the indicator pH. If the sample pH is higher than the indicator pH (≈ 7.6 pH units) the pH perturbation will be negative and vice versa if the sample pH is less than the indicator solution. The relatively small error observed between the UV-VIS spectrophotometer and ALpHI indicates that highly reproducible pH measurements are possible if the pH perturbation caused by CR is minimized.

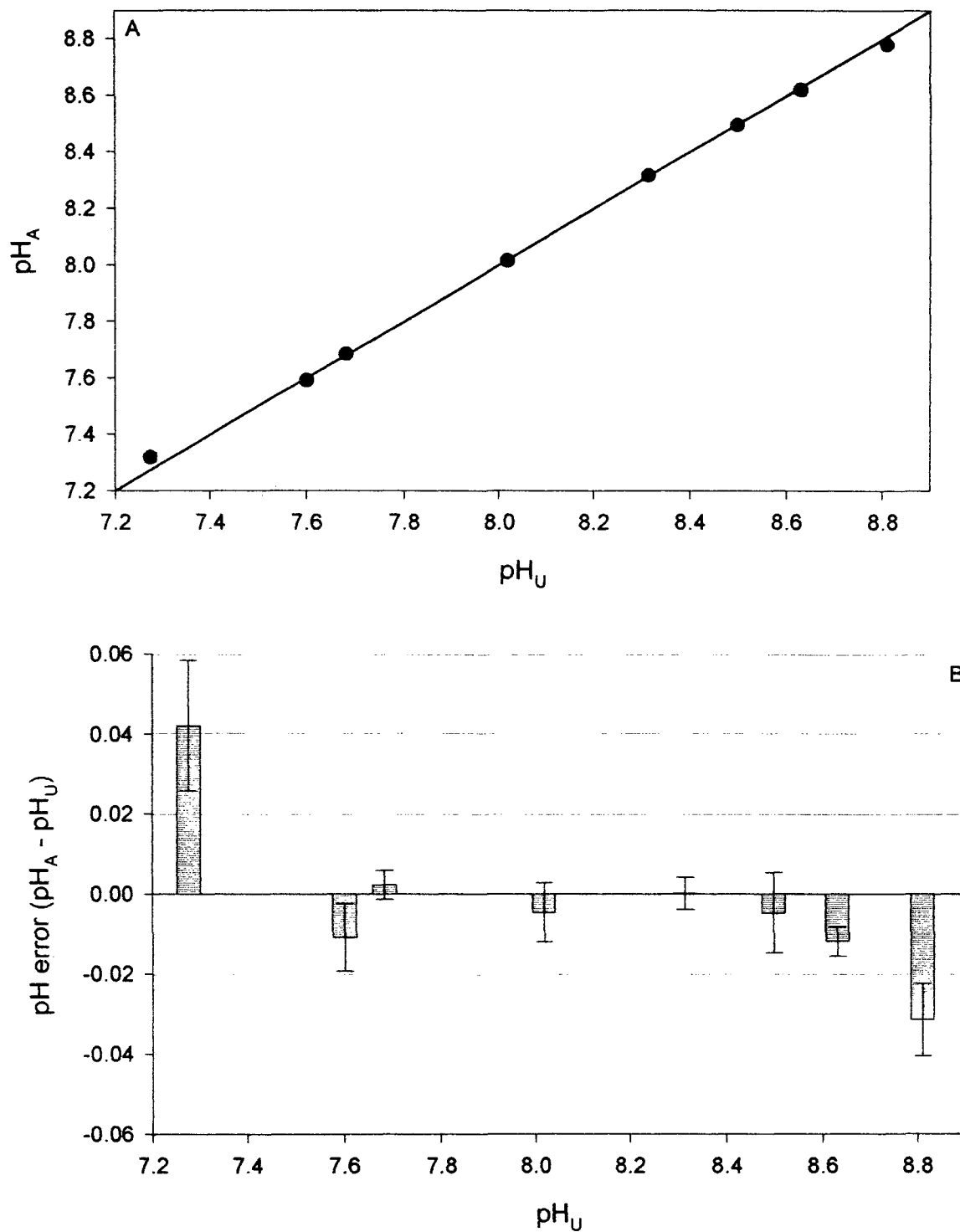


Figure 4-3. The results of the H_3BO_3 and KH_2PO_4 buffer reproducibility experiment. A. The black line is a 1:1 line. B. pH error represents the difference between pH_A and pH_U .

4.2 Freshwater Relative Accuracy Experiments

The relative accuracy of ALpHI with respect to the UV-VIS spectrophotometer was also determined using freshwater samples in a 0.75 cm pathlength fiber-optic flow cell. Absorbance and temperature were measured and pH was determined for the ALpHI using Equation 6. Results of sample 111998a have been provided as examples (Figures 4-4 and 4-5). Absorbance and temperature data from Figure 4-4 were used to calculate pH with Equation 6. The pH, without temperature adjustments is shown in Figure 4-4C with 3σ error bars. Typical 3σ levels for the freshwater samples were $\pm 0.001 - 0.004$ pH units. The UV-VIS spectrophotometer temperature for sample 111998a was set at 20.50°C ; therefore the pH_A was adjusted to 20.50°C for the graphs in Figure 4-5 by applying the slope, $-0.011 \text{ pH units } ^\circ\text{C}^{-1}$, from Figure 3-12. Temperature adjusted pH_A are used so that the relationship between pH_A and pH_U can be more easily evaluated.

Sample 111998a provides an interesting example of the relationship between pH and [CR] (Figure 4-5A). As the concentration of CR varies between $7.5 \times 10^{-6} \text{ M}$ and $1.6 \times 10^{-5} \text{ M}$, the pH appears to mirror the [CR] variations. The strong correlation between pH and [CR] is confirmed in Figure 4-5B.

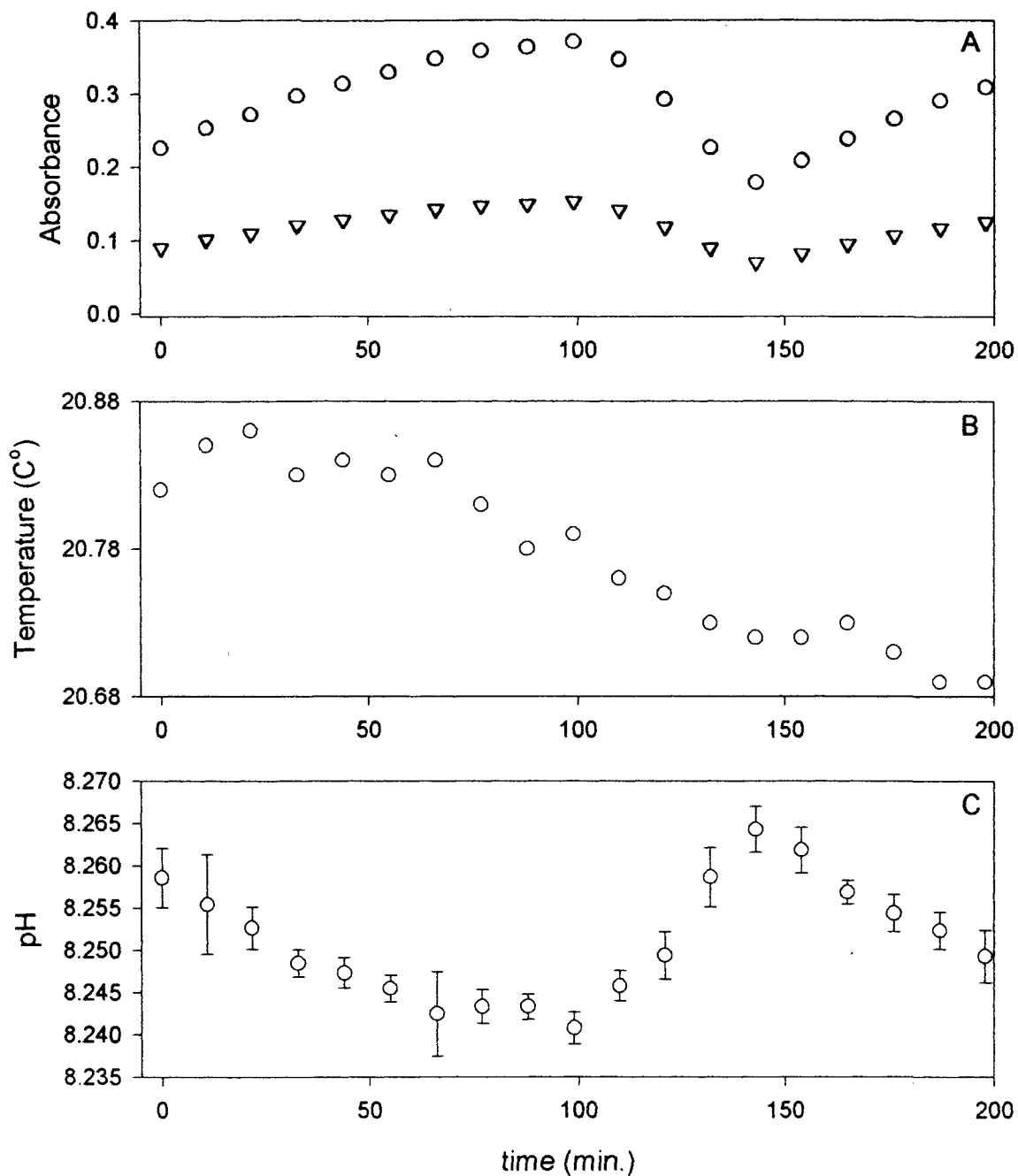


Figure 4.4. Data recorded from a sample of freshwater with the 0.75 cm flow cell (sample 111998a). A. Clusters of absorbance measurements, ○ = 577 nm and ▽ = 439, are overlying data points from each measurement cycle. B. Temperature measurements. C. ALPHI pH measurements with 3σ error bars. $\text{pH}_u = 8.291$.

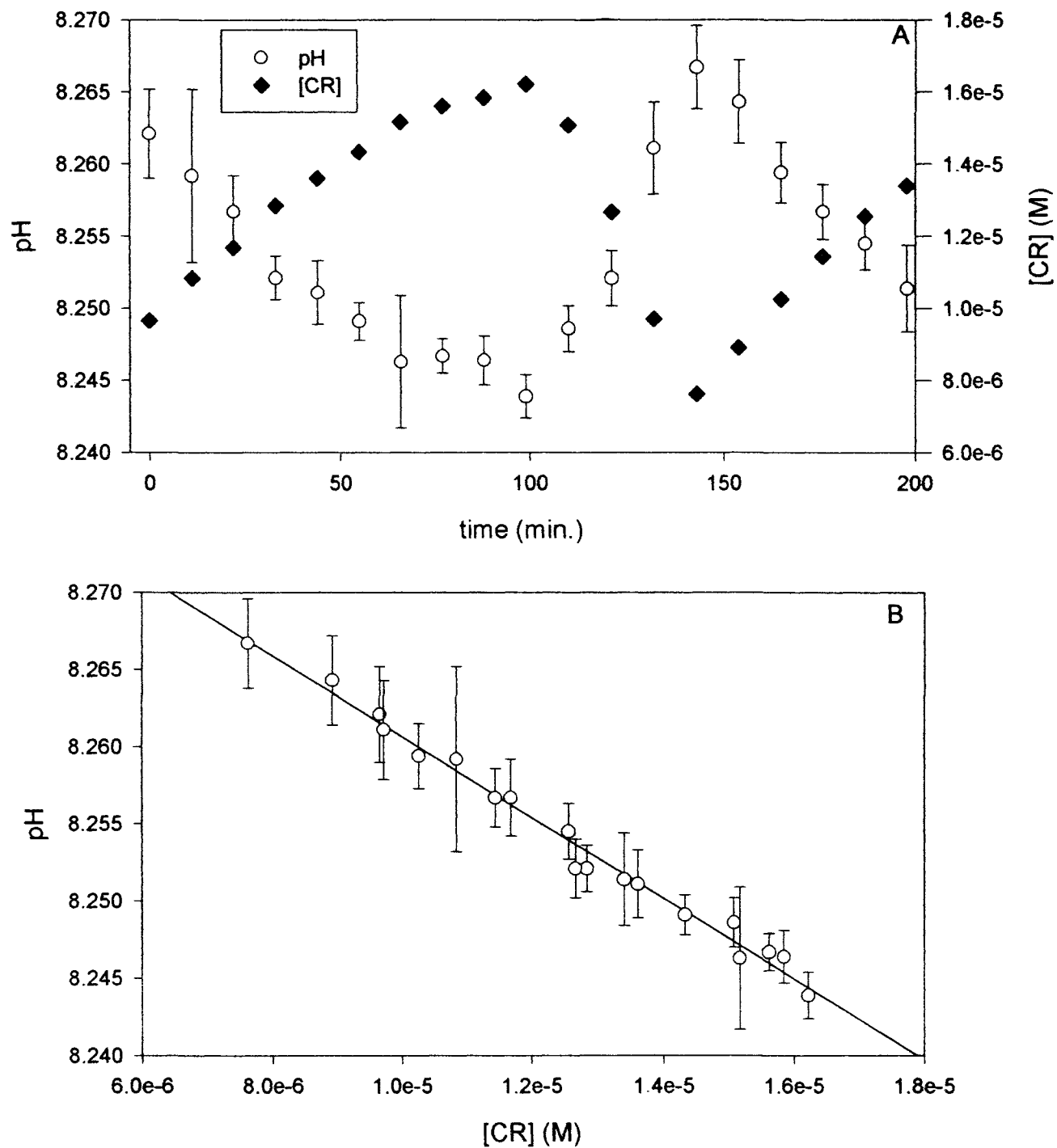


Figure 4-5. Temperature-adjusted pH_A measurements of the freshwater sample 111998a with the 0.75 cm flow cell. Graphs A and B were used to determine the correlation between pH and [CR], the regression line in graph B is $\text{pH} = 8.2868 - 2613[\text{CR}]$, $r^2 = 0.987$. $\text{pH}_U = 8.291$.

Ten freshwater samples, including 111998a, with varying pH (7.4 – 8.6) were analyzed. The relative accuracy of the ALpHI was determined by comparing temperature corrected pH_A to pH_U for the same sample. Figure 4-6 compares the correlation of these results to a 1:1 line, while Table 4-1 shows the error for each sample as $pH_A - pH_U$. Each circle in Figure 4-6 represents an average pH_A ($n = 8$) for one sample. Freshwater relative accuracy results are presented in a table rather than a bar graph (as used for the buffer solutions) because the freshwater samples do not show a significant trend (not measured over a large enough pH range). Figure 4-5B illustrates that freshwater pH is more dependent on $[CR]$ (slope = $-2613 \text{ pH units } [CR]^{-1}$) than the buffer pH was in Figure 4-2 (slope = $654.4 \text{ pH units } [CR]^{-1}$). Therefore, the average error was determined for each freshwater sample by selecting data for which $[CR]$ was close to $2.0 \times 10^{-5} \text{ M}$.

The series of freshwater samples ranging in pH from 7.4 to 8.5 pH units provided insights into the limitations of ALpHI. The relative accuracy throughout the observed pH range was $\sim 0.04 - 0.07$ pH units, well outside our projected goal of < 0.01 pH units. Consequently, we hypothesized, if we could find a way to reduce the concentration of CR in the sample, while maintaining a reasonable absorbance, we could improve the relative accuracy of ALpHI.

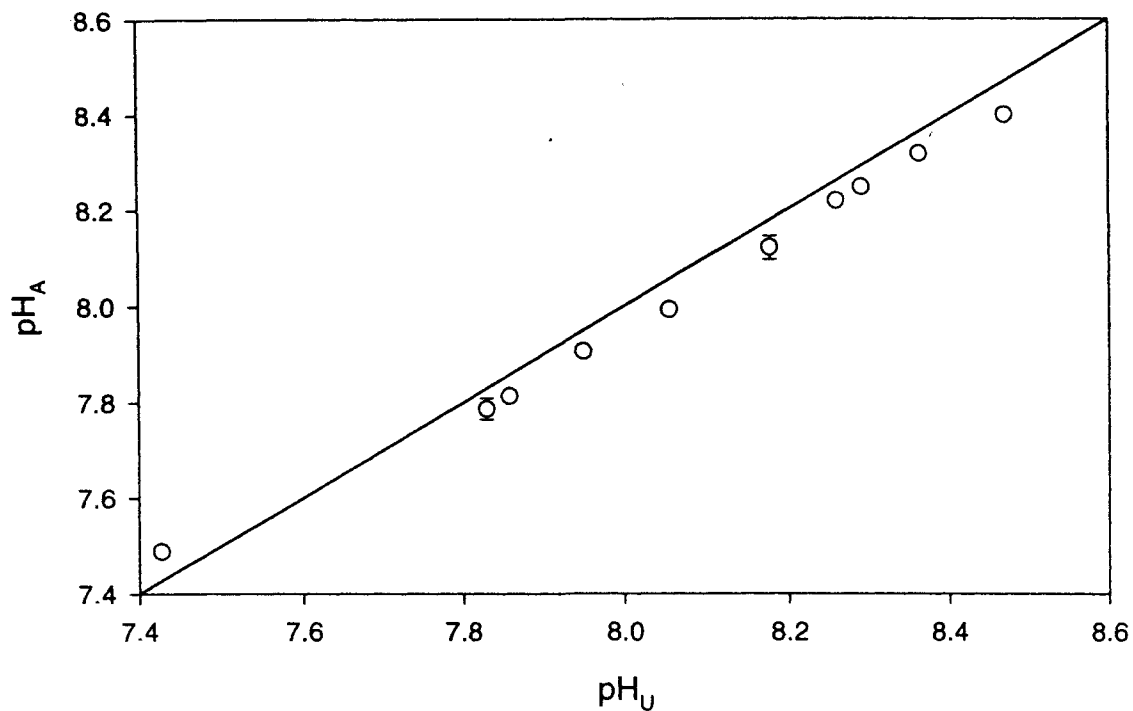


Figure 4-6. The comparison of pH_A to pH_U for freshwater samples in the 0.75 cm fiber-optic flow cell. Error bars represent 3σ for one sample; circles with no visible error bars have small 3σ . The black line is 1:1.

Table 4-1. The average error for each freshwater, 0.75 cm cell sample was determined by the equation $pH_A - pH_U$.

sample	pH_U	avg. error	avg. [CR] (M)
112398b	8.470	-0.068	2.47E-05
112398a	8.363	-0.046	2.15E-05
111998a	8.291	-0.045	1.54E-05
110298a	8.260	-0.041	1.70E-05
102998a	8.178	-0.057	1.93E-05
110598a	8.056	-0.063	2.00E-05
110598b	7.950	-0.043	1.87E-05
110798a	7.858	-0.044	2.00E-05
110398b	7.830	-0.043	1.81E-05
110698a	7.428	0.060	1.96E-05

In order to reduce the concentration of CR while maintaining reasonable absorbance measurements we switched to 2.0 cm pathlength optical flow cell. Since the pathlength was increased by 267%, we should be able decrease [CR] by 38%. The longer pathlength, however, severely decreased the light throughput because more light is scattered out of the cell. Therefore, we also replaced the 400 μm core fiber-optic cables with 600 μm core fiber-optic cables and the throughput increased back to reasonable levels (approximately 1.20 V for the reference channel). Again freshwater samples were prepared and analyzed to evaluate ALpHI relative accuracy

The same portfolio of graphs was also constructed for the new freshwater samples (sample 011899c is used as an example) in which a 2.0 cm pathlength fiber-optic flow cell was used. Figure 4-7 demonstrates that consistent pH can be obtained from these relatively consistent absorbances and temperatures. Typical 3σ levels for the freshwater samples in Figure 4-7C are $\pm 0.002 - 0.004$ pH units. CR concentrations were successfully reduced to approximately 4.5×10^{-6} M, which is quite an improvement over the 2.0×10^{-5} M CR that was associated with most measurements which utilized the 0.75 cm pathlength flow cell. Although the pH [CR]⁻¹ slope is higher (-7228 pH units [CR]⁻¹) compared to previous freshwater measurements (-2613 pH units [CR]⁻¹), the pH [CR]⁻¹ correlation is much weaker ($r^2 = 0.54$) due to the small concentration range in Figure 4-8B. A small temperature-adjustment was applied to pH_A data in Figure 4-8 in order to agree with the UV-VIS spectrophotometer temperature (21.00°C).

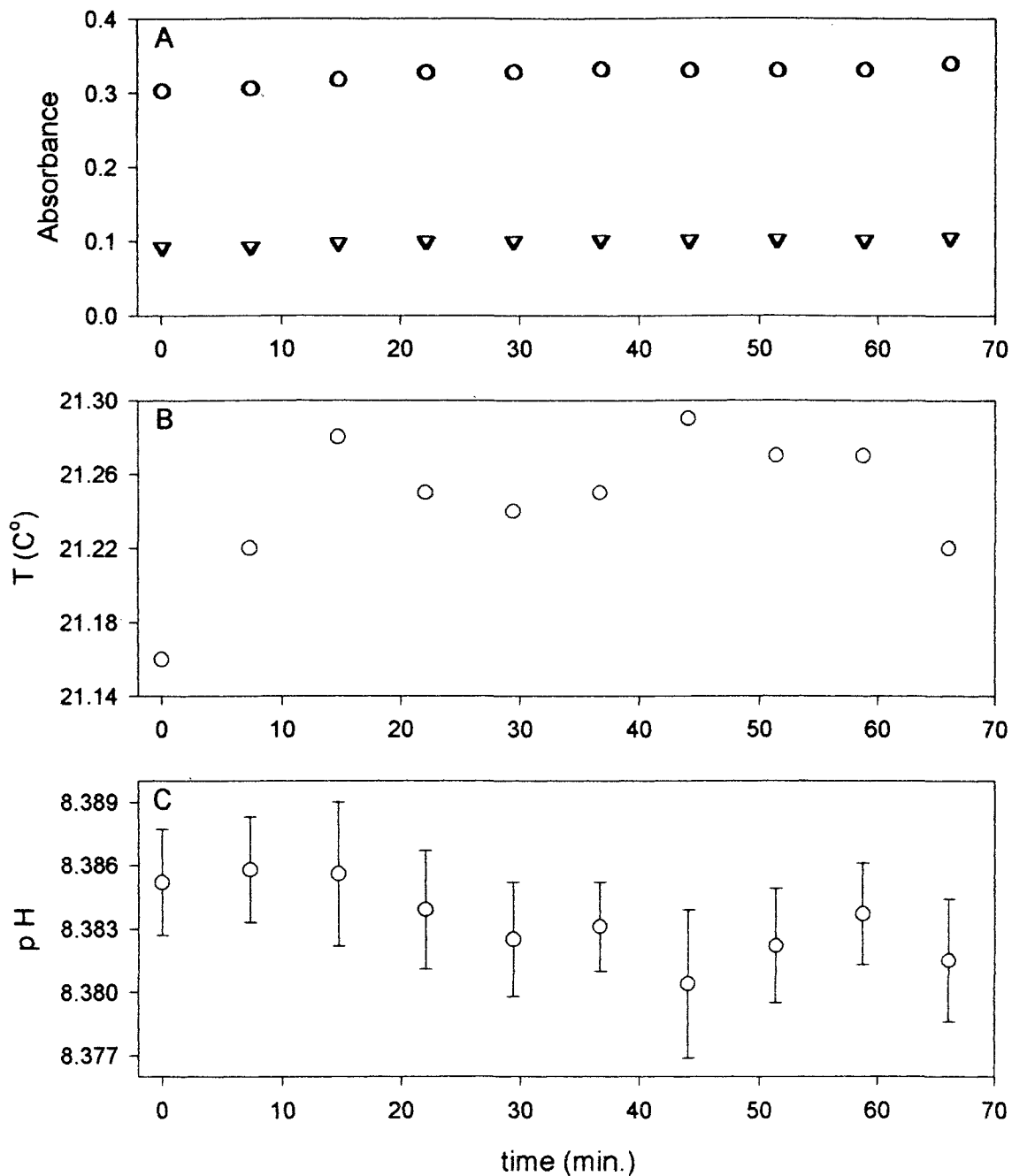


Figure 4-7. Data recorded from a sample of freshwater using the 2.0 cm optical flow cell (sample O11899c). A. Clusters of absorbance measurements, ○ = 577 nm and ▽ = 439, are overlying data points from each measurement cycle. B. Temperature measurements. C. ALpHI pH measurements with 3σ error bars. $\text{pH}_U = 8.394$.

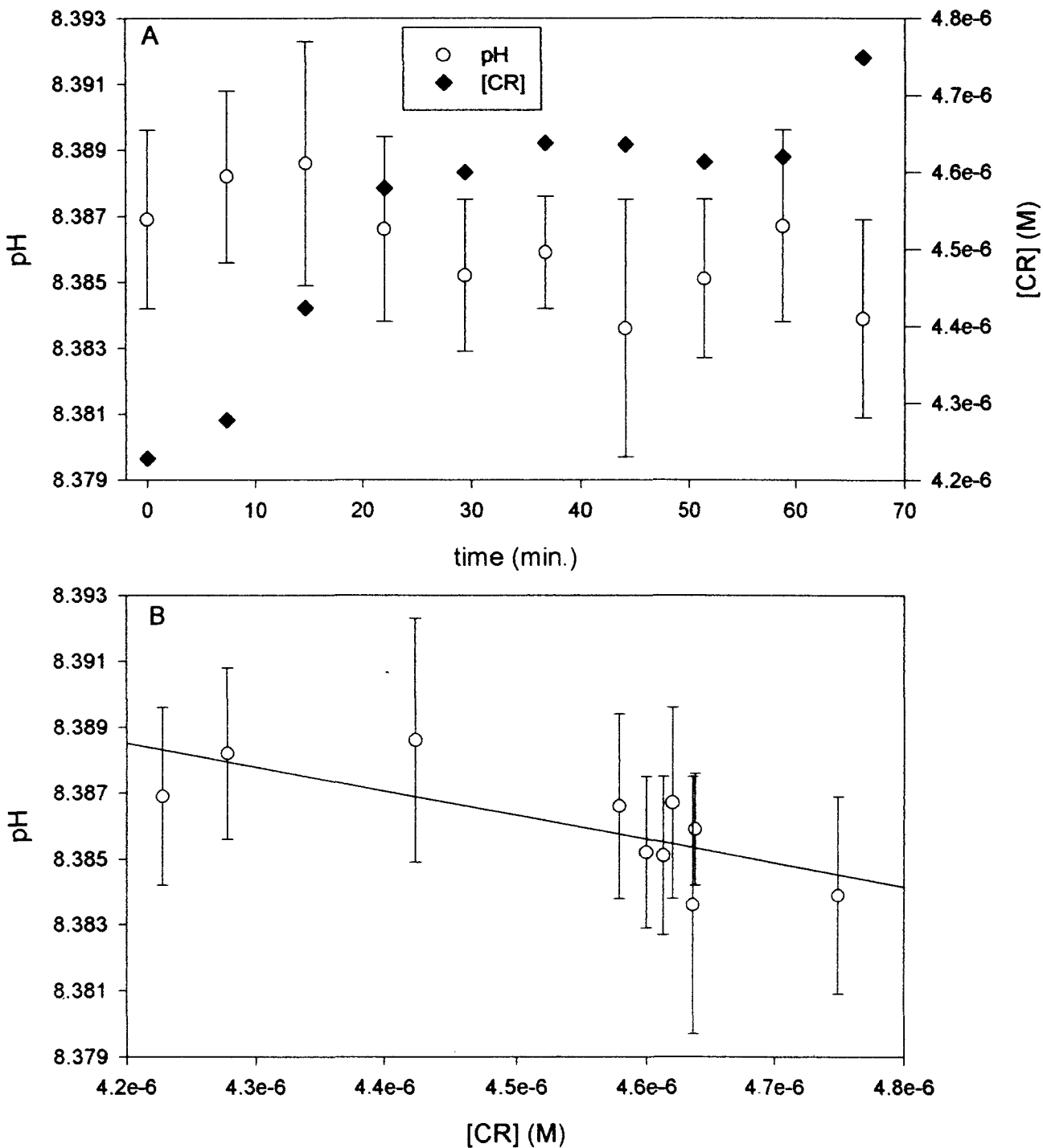


Figure 4-8. Temperature-adjusted pH_A measurements of the freshwater sample O11899c with the 2.0 cm optical flow cell. Graphs A and B were used to determine the correlation between pH and [CR], the regression line in graph B is $pH = 8.4189 - 7228[CR]$, $r^2 = 0.54$. $pH_U = 8.394$. pH_A temperature was adjusted to 21.00°C.

The freshwater reproducibility experiment with the 2.0 cm pathlength optical flow cell consisted of 12 samples ranging from 7.8 – 8.5 pH units. Figure 4-9 and Table 4-2 presents these results in the same format as the previous freshwater results. Overall, the results were very pleasing; we met our goal of reducing the relative accuracy to < 0.01 . The best working range for CR, however, is unclear and further studies should be conducted to characterize the limits of the indicator more thoroughly in freshwater

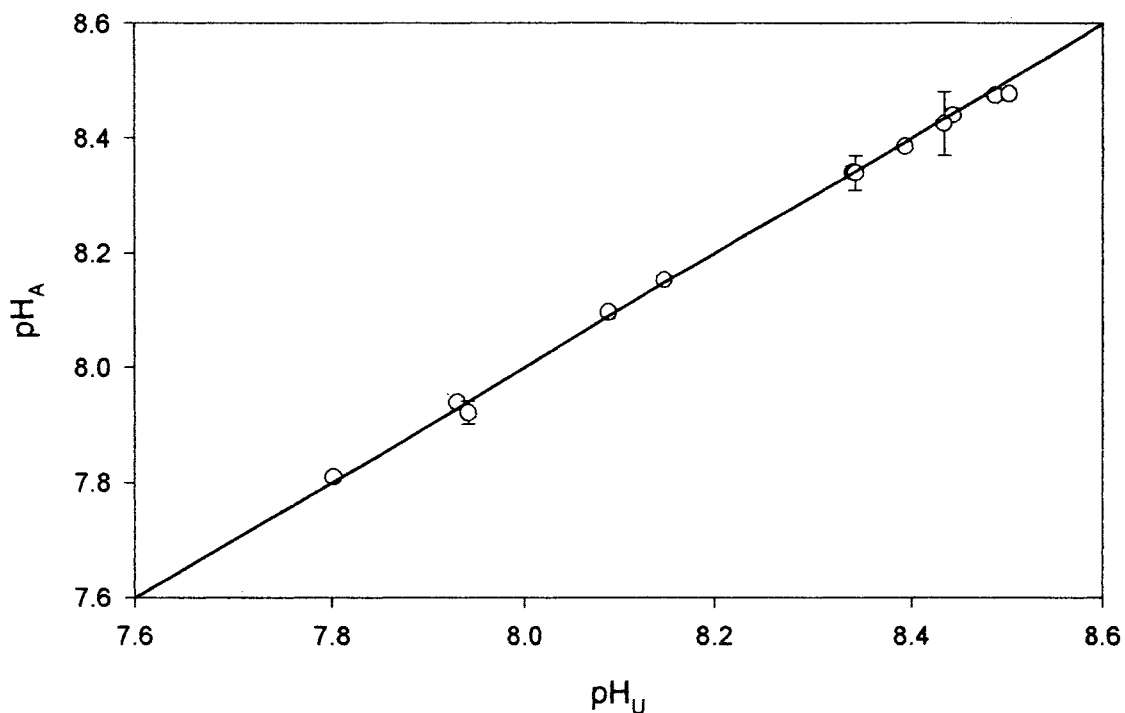


Figure 4-9. The comparison of pH_A to pH_U for freshwater samples in the 2.0 cm pathlength fiber-optic flow cell. Error bars represent 3σ for one sample; circles with no visible error bars have small 3σ . The black line is 1:1.

Table 4-2. Error ($\text{pH}_A - \text{pH}_U$) recorded while using the 2.0 cm fiber-optic flow cell.

sample	pH_U	error	[CR] (M)
012099a	8.501	-0.025	5.19E-06
012199a	8.487	-0.012	5.44E-06
012199b	8.443	-0.004	6.67E-06
011299b	8.434	-0.010	6.27E-06
011899c	8.394	-0.008	4.59E-06
011899a	8.343	-0.003	4.18E-06
011899b	8.340	0.002	2.53E-06
011499a	8.1494	0.004	4.92E-06
011399b	8.091	0.006	4.52E-06
011299d	7.941	-0.018	4.28E-06
011399a	7.930	0.010	5.65E-06
010499a	7.802	0.007	7.92E-06

Chapter 5

Discussion

5.1 Relative Accuracy

Initial ALpHI measurements (which were not described in the relative accuracy study just presented) were as much as 0.20 pH units less than the value measured on the UV-VIS spectrophotometer. Consequently, there have been many manipulations involving ALpHI, the indicator, and the operating program in order to overcome earlier setbacks. Utilizing the 2.0 cm pathlength optical flow cell in the latest relative accuracy experiments allowed us to minimize indicator pH perturbations. Table 5-1 offers a comparison of the results for eight representative samples from the relative accuracy experiments to further emphasize the improvement obtained.

Table 5-1. The table summarizes relative accuracy results for representative samples.

sample	pH _U	Relative accuracy pH _A - pH _U	[CR] (M)
100798a♦♥	8.018	-0.004	2.00×10^{-5}
100798b♦♥	8.498	-0.005	1.91×10^{-5}
111998a♣♥	8.291	-0.045	1.54×10^{-5}
110398b♣♥	7.830	-0.043	1.81×10^{-5}
112938b♣♥	8.470	-0.068	2.47×10^{-5}
011899c♣♠	8.394	-0.008	4.59×10^{-6}
011499a♣♠	8.150	0.004	4.92×10^{-6}
011399a♣♠	7.930	0.010	5.65×10^{-6}

♦ buffer solution, ♣ freshwater sample, ♥ 0.75 cm cell, ♠ 2.0 cm cell

5.2 ALpHI Precision

ALpHI pH precision was defined as 3σ for one cycle ($n= 8$). During an individual cycle, both the CR / sample solution ratio and temperature remain relatively stable, which resulted in consistently high precision. Calculated and measured ALpHI precisions are reported for representative samples in Table 5-2 to further illustrate this point. Propagating the 3σ absorbance uncertainty ($n = 8$) produced relative uncertainties of R values for each cycle. The percent relative uncertainty of R listed below represents an average for eight cycles for each sample. Minimum and maximum R values were determined and plugged into Equation 6 to calculate the pH uncertainties. Regardless of the sample or cell pathlength, the precision is constantly between ± 0.0034 and ± 0.0016 .

Table 5-2. The measured and calculated precision of ALpHI are listed below, $n = 8$.

sample	pH _U	R % relative uncertainty	Calculated pH uncertainty	Measured pH 3σ precision
100798a♦♥	8.018	0.41%	0.0019	0.0017
100798b♦♥	8.498	0.59%	0.0030	0.0028
111998a♣♥	8.291	0.82%	0.0039	0.0034
110398b♣♥	7.830	0.73%	0.0033	0.0024
112938b♣♥	8.470	0.32%	0.0016	0.0016
011899c♣♠	8.394	0.59%	0.0029	0.0028
011499a♣♠	8.150	0.55%	0.0026	0.0028
011399a♣♠	7.930	1.16%	0.0052	0.0033

♦ buffer solution, ♣ freshwater sample, ♥ 0.75 cm cell, ♠ 2.0 cm cell

5.3 Optimal Response Characteristics of ALpHI

ALpHI's optimal response characteristics are reported for studies with the 2.0 pathlength fiber-optic flow cell.

Table 5-3. Optimal response characteristics.

Characteristic	Description	Result
<u>Dynamic range</u>	The working range of the indicator.	7.6 – 8.6 pH units
<u>Response time</u>	Time required to detect 90% of a pH change (flow rate = 50 $\mu\text{L min}^{-1}$).	~50 minutes
<u>Flush time</u>	Time required to completely flush the plumbing system of all indicator (with the Neptune Research valve).	80 minutes
<u>Indicator consumption</u>	Assuming 5.0 μM CR (which provides optimal absorbances).	6.5 mL of 0.020 M CR yr^{-1}
<u>Relative accuracy</u>	The reproducibility between ALpHI and the UV-VIS spectrophotometer over the dynamic range (given as the absolute value of the average of the pH error in Table 4-2) (n = 10).	± 0.008 pH units
<u>Precision</u>	The 3σ precision of one measurement cycle (n = 8).	$\pm 0.001 - \pm 0.004$ pH units

5.4 Freshwater pH Perturbation

The ability to successfully model the pH perturbation of freshwater caused by the indicator would allow us to produce results closer to the true pH. However, this proved to be a most difficult task. We propose that the large discrepancy illustrated in Figure 3-6 and Table 3-3 are caused by the 5% of impurities in the sodium salt indicator. We attempted to purify 95% pure CR (not from sodium salt), however, our results indicate that we did not significantly alter the pH perturbation. If a theoretical method cannot be produced, an empirical solution could be developed based the alkalinity that would cause the observed pH perturbation.

Chapter 6

Conclusions

6.1 Summary of Results

Our operational goals for ALpHI which include a relative accuracy better than ± 0.01 pH units and a precision better than ± 0.005 pH units, have been accomplished. Unlike electrodes, ALpHI is capable of highly reproducible pH measurements over an extended period without calibrations. Although an in situ version of ALpHI has not yet been constructed, the relative accuracy and precision that ALpHI has displayed with the 2.0 cm pathlength flow cell should lead to its successful development.

6.2 Future Applications

Now that the performance characteristics have been sufficiently optimized, an in situ pH sensor can be prepared for deployment in the Clark Fork River. An existing housing from a similar in situ instrument, SAMI-CO₂ (DeGrandpre et al. 1995) will be converted to house the in situ pH sensor. When the instrument is ready for deployment, a site will be selected on the Clark Fork River. Spectrophotometric analysis of water samples from the test site will be completed several times per day during the deployment period. The success of this fieldwork would open the door for other applications such as monitoring of water treatment sites and mine tailings.

Since the pH of acid mine tailings can fluctuate over a larger range, other indicators could be characterized to find a more compatible fit. Possibly, multiple ALpHIs could be deployed simultaneously with different indicators. An array of indicators such as CR (7.2 – 8.8), bromocresol purple (5.2 – 6.8), and congo red (3.0 –

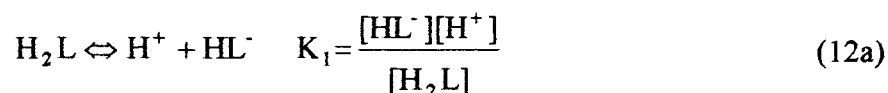
5.0) could be deployed. Such an undertaking would require advanced knowledge of the study site pH range and the characteristics of several indicators.

Development of a spectrophotometric in situ pH instrument will enhance the abilities of investigators to acquire more frequent pH measurements than previously possible by grab sampling techniques. Investigators will also be able to avoid the drift and reproducibility problems of electrodes. Long-term deployments of an in situ pH instrument would provide a more complete time series of diel, episodic, and seasonal fluctuations of pH that would have many applications. Any investigations of freshwater chemistry, such as acidification, inorganic carbon cycling or geochemical trends, would be improved by a more accurate pH time series.

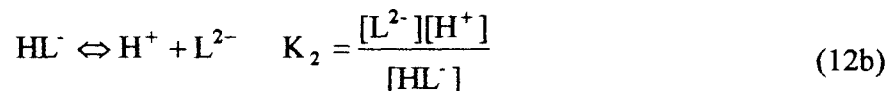
Appendix I

Derivation of Equation 6

The derivation of Equation 6 from Beer's Law and the Henderson-Hasselbalch equation was first presented by Clayton and Byrne (1993). The chemical equilibria among the three forms: H_2L , HL^- , and L^{2-} can be described by the dissociation constants:



and



where [] denotes concentration. Total indicator concentration, $L_T = [H_2L] + [HL^-] + [L^{2-}]$, can be expressed in terms of K_1 and K_2 .

$$L_T = [L^{2-}] \left(\frac{[H^+]^2}{K_1 K_2} + \frac{[H^+]}{K_2} + 1 \right) \quad (13)$$

The absorbance due to L in solution is described as:

$$A_\lambda = (\epsilon_{H_2L\lambda}[H_2L] + \epsilon_{HL\lambda}[HL^-] + \epsilon_{L^{2-}\lambda}[L^{2-}])b \quad (14)$$

where A_λ is the absorbance at wavelength λ , $\epsilon_{x\lambda}$ is molar absorptivity of species x at wavelength λ , and b is the optical pathlength. Equation 14 can be transformed into:

$$\frac{A_\lambda}{b} = [L^{2-}] \left(\epsilon_{H_2L\lambda} \frac{[H^+]^2}{K_1 K_2} + \epsilon_{HL\lambda} \frac{[H^+]}{K_2} + \epsilon_{L^{2-}\lambda} \right) \quad (15)$$

By introducing the variable $a_\lambda = A_\lambda / (b L_T)$ and dividing Equation 15 by Equation 13 we obtain:

$$a_\lambda = \frac{A_\lambda}{bL_T} = \frac{[L^{2-}] \left(\epsilon_{H_2L\lambda} \frac{[H^+]^2}{K_1 K_2} + \epsilon_{HL\lambda} \frac{[H^+]}{K_2} + \epsilon_{L^{2-}\lambda} \right)}{[L^{2-}] \left(\frac{[H^+]^2}{K_1 K_2} + \frac{[H^+]}{K_2} + 1 \right)} \quad (16)$$

Since we are interested in a freshwater system with a pH of approximately 8.0, we can assume that $[H_2L] = 0$. Therefore, the H_2L terms drop out to give:

$$a_\lambda = \frac{A_\lambda}{bL_T} = \frac{[L^{2-}] \left(\epsilon_{HL\lambda} \frac{[H^+]}{K_2} + \epsilon_{L^{2-}\lambda} \right)}{[L^{2-}] \left(\frac{[H^+]}{K_2} + 1 \right)} \quad (17)$$

The ratio of indicator absorbances, $R = A_{577} / A_{439}$, can be written as a_{577} / a_{439} from Equation 17:

$$R = \frac{A_{577}}{A_{439}} = \frac{\epsilon_{HL\ 577} \frac{[H^+]}{K_2} + \epsilon_{L^{2-}\ 577}}{\epsilon_{HL\ 439} \frac{[H^+]}{K_2} + \epsilon_{L^{2-}\ 439}} \quad (18)$$

If Equation 18 is algebraically manipulated and divided by $\epsilon_{HL\ 439}$, we obtain:

$$\frac{R[H^+]}{K_2} + \frac{\epsilon_{L^{2-}\ 439} R}{\epsilon_{HL\ 439}} = \frac{\epsilon_{HL\ 577} [H^+]}{\epsilon_{HL\ 439} K_2} + \frac{\epsilon_{L^{2-}\ 577}}{\epsilon_{HL\ 439}} \quad (19)$$

Since:

$$e_1 = \frac{\epsilon_{\text{HL } 577}}{\epsilon_{\text{HL } 439}} \quad e_2 = \frac{\epsilon_{\text{L}^{2-} 577}}{\epsilon_{\text{HL } 439}} \quad e_3 = \frac{\epsilon_{\text{L}^{2-} 439}}{\epsilon_{\text{HL } 439}} \quad (20)$$

and

$$\frac{[\text{H}^+]}{K_2} = \frac{[\text{HL}^-]}{[\text{L}^{2-}]} \quad (21)$$

we are able to obtain:

$$\frac{[\text{L}^{2-}]}{[\text{HL}^-]} = \frac{R - e_1}{e_2 - Re_3} \quad (22)$$

Resulting in:

$$\text{pH} = \text{pK}_a + \log \left(\frac{R - e_1}{e_2 - Re_3} \right) \quad (6)$$

Appendix II

CRTURB.BAS

***** Theoretical Calculations Program *****

' Version 3.0

' CRAIG M. FRENCH

' NOTE: This program will calculate the pH and alkalinity for
' user supplied variables and assumes equilibrium. This program
' is adapted from Mike DeGrandpre's program that predicts the
' equilibrium response of a fiber optic absorbance sensor
' to a range of aqueous CO2 concentrations.

' Version 1.0 to 1.1 --> Changed pKa equation. (07/21/97)

' Version 1.1 to 2.0 --> Included BTB in alkalinity & pH equations.(01/8/98)

' Version 3.0 --> BTB was replaced by CR (11/09/98)

' NOTE: How do we calculate an appropriate offset (activity coefficients)
' to the BTB pKa equation? Remember that we found the pKa with a
' buffer of ionic strength = 0.0235 M. Does the extended Debye-
' Huckel equation work well for large organic anions like BTB?
' If so, what do we use for its effective hydrated radius?
' We've decided that our earlier estimates may be inappropriate.
' Therefore, we will not correct the pKa for activity until we can
' find answers to these questions. (04/24/98)

**

DIM Ct(400), XB1(10), XB2(10), pH(400), ADF(400)

CLS

pH1 = 0: pH2 = 14: H1 = 10 ^ (-pH1): H2 = 10 ^ (-pH2)

INPUT "What is the total carbon(moles/Liter)"; Ct

INPUT "Temp(C)"; T

INPUT "Input the indicator concentration (moles/Liter) . ", HIT

INPUT "Input the alkalinity (moles/Liter) : ", B

INPUT "Would you like to save the output? (Y or N) : ", Ans\$

```
Answer$ = UCASE$(Ans$)
```

```
IF Answer$ = "Y" THEN
INPUT "Input filename for output ", Out$
ELSE
END IF
```

```
T1 = T + 273.15 'Absolute Temp. (K)
```

```
REM Note that "LOG(x)" in QB45 is actually "ln(x)" so need to divide by LOG(10)!
REM The pKa eqn. below was determined using low ionic strength buffers by French.
```

```
pKa = (865 1 / T1) + 2.092 + (1.3 * LOG(T1) / LOG(10))
Ka = 10 ^ (-pKa)
```

```
***K1 and K2 are Millero's dissociation consts. for H2CO3 at S=0 (Goyet,'89)
```

```
K1 = 10 ^ (-(6320.81 / T1 - 126.3405 + 19.568 * LOG(T1)))
K2 = 10 ^ (-(5143.69 / T1 - 90.1833 + 14.613 * LOG(T1)))
Kw = 10 ^ ((-4470.99 / T1 + 6.0875 - .01706 * T1))
```

```
DF = HIT / 00188 'DF is the dilution factor
```

```
*****
```

```
GOSUB BRACKET
GOSUB NTSAFE
```

```
*****
```

```
IF Answer$ = "Y" THEN
```

```
OPEN Out$ FOR OUTPUT AS #1
```

```
PRINT #1, "Ct", "pH", "Final Alk", T, HIT, B
```

```
PRINT ""
```

```
PRINT "Ct", "pH", "Alkalinity"
```

```
PRINT #1, Ct, pH, USING "#.#####^~^~ "; ADF
```

```
PRINT Ct, pH, ADF
```

```
CLOSE #1
```

```
ELSE
```

```
PRINT ""
```

```
PRINT "pH", "Alkalinity"
```

```
PRINT pH, ADF
```

```
PRINT ALF1I, ALF2I, ALF0I
```

```
END IF
```

```
END
```

```
***** Bracketing Function *****
```

```
BRACKET
```

```
  pH1 = 0: pH2 = 14
```

```
  N = 30          'N = number of segments between H2 and H1
```

```
  NBB = 3        'NBB = maximum # of roots sought
```

```
  NB = 0
```

```
  pH = pH1       'pH2 and pH1 = high and low pH estimates
```

```
  DpH = (pH2 - pH1) / N 'interval to test for zero crossing
```

```
  GOSUB FUNC1    'calculate for low pH value
```

```
  FP = FSUM
```

```
  FOR K = 1 TO N 'find roots over N intervals
```

```
    pH = pH + DpH 'increments pH
```

```
    GOSUB FUNC1  'calculate again and check for zero crossing
```

```
    FC = FSUM
```

```
    IF FC * FP < 0 THEN
```

```
      NB = NB + 1
```

```
      XB1(NB) = pH - DpH
```

```
      XB2(NB) = pH
```

```
    END IF
```

```
    FP = FC
```

```
    IF NBB = NB THEN RETURN
```

```
  NEXT K
```

```
  pH1 = XB1(1): pH2 = XB2(1) 'sets range for bisection
```

```
  RETURN
```

```
***** Bisection Convergence Method *****
```

```
NTSAFE:
```

```
  XACC = 00000000001# 'sets convergence limit
```

```
  pH = pH1: GOSUB FUNC1 F = FSUM
```

```
  pH = pH2: GOSUB FUNC1 FMID = FSUM
```

```
  IF F * FMID > 0 THEN PRINT "ERROR. Root must be bracketed" END
```

```
  IF F < 0 THEN 'orient search so that f(x) < 0
```

```
    RTBIS = pH1
```

```
    DpH = pH2 - pH1
```

```

ELSE
  RTBIS = pH2
  DpH = pH1 - pH2
END IF

MAXIT = 100
FOR J = 1 TO MAXIT
  DpH = 5 * DpH
  pHMID = RTBIS + DpH
  pH = pHMID: GOSUB FUNC1. FMID = FSUM
  IF FMID <= 0 THEN RTBIS = pHMID
  IF ABS(DpH) < XACC THEN RETURN
NEXT J

RETURN

'***** Calculate New Values *****
FUNC1

  H = 10 ^ (-pH)
  CtDF = Ct * (1 - DF)
  ALF2 = (H ^ 2 / K1 / K2 + H / K2 + 1) ^ -1
  ALF1 = (H / K1 + 1 + K2 / H) ^ -1
  ALF2I = (H ^ 2 / (Ka * .01) + H / Ka + 1) ^ -1
  ALF1I = (H / 01 + 1 + Ka / H) ^ -1
  ALF0I = (1 + 01 / H + Ka * 01 / H ^ 2) ^ -1
  ADF = B * (1 - DF)
  X = ALF1 * CtDF + 2 * ALF2 * CtDF + HIT * ALF2I - ADF
  FSUM = -H ^ 2 + X * H + Kw
RETURN

END

```

Appendix III

ALPHI1.TT4

ALPHI1.TT4 is the operating program for ALpHI which was adapted from SAMI.TT4 written by Steve Smith and Michael DeGrandpre.

```

3 REM  FILE ALPHI1 TT4 MODIFIED BY CMF 1/23/99
4 REM  (This is the latest ALpHI version for model 4 and above)
,
5 REM  *****
10 REM GOTO 2000 (DATA DUMP), 3000 (SET CLOCK, DATA COUNTER)
15 REM I/O(0) = LAMP POWER      I/O(1) = DETECTOR +/- 12V SUPPLY
20 REM I/O(7) = WATER PUMP     I/O(14) = VALVE CONTROL
25 REM I/O(15) =                I/O(5,9,10,11) CLOCK CONTROL
30 REM CHAN(0) = EXT SENSOR #1  CHAN(1) = 724 nm (RED)
35 REM CHAN(2) = 577 nm (GREEN) CHAN(3) = 439 nm (BLUE)
40 REM CHAN(4) = BATTERY VOLTS  CHAN(5) = BATTERY VOLTS
45 REM CHAN(6) = EXT SENSOR #2  CHAN(7) = TEMPERATURE
50 REM A-N are VARIABLES      P-Z are INDICES/COUNTERS
57 REM 36 BYTES ARE SAVED PER MEASUREMENT CYCLE
60 REM  *****
,
65 ONERR 8000: REM ERROR TRAP FOR CLOCK DATA TRANSFER ERROR
70 ASM &H9A, DW 8 . REM 512K MEMORY EXPANSION
75 FOR R = 0 TO 15: PCLR R: NEXT R. REM SHUT DOWN ALL DEVICES
80 GOSUB 4000: REM GET TIME FROM RTC, RELOAD TATTLETALE
95 GOTO 200: REM START MEASUREMENT
,
97 REM *****CTRL-C DESTINATION*****
100 FOR R = 0 TO 15: PCLR R. NEXT R. REM SHUT DOWN ALL DEVICES
110 ASM &HBB, DB &H0A. C = CHAN(0): REM SHUT OFF A/D CONVERTER
120 STOP
,
200 REM ***** START OF MEASUREMENT SEQUENCE*****
215 FOR R = 0 TO 15: PCLR R. NEXT R. REM CLEAR ALL I/Os
230 GOSUB 1000
255 GOTO 65
260 DONE
,
1000 REM ***** MEASUREMENT SEQUENCE *****
1300 REM ***** I-PULSE *****
1301 RTIME: REM *GET TIME*
```

```
1303 PRINT #02,?(4),"",?(3),"",?(5)
1305 PSET14:SLEEP0:SLEEP10
1310 PSET7:SLEEP0:SLEEP1:PCLR14
1315 SLEEP0:SLEEP200:PCLR7:REM *WATER PUMP*
1320 FOR R = 1 TO 60: REM *WAIT 60 SECONDS*
1325 SLEEP 0: SLEEP 100
1330 NEXT R
1335 FOR S = 1 TO 10: REM *NUMBER OF SAMPLE PULSES*
1340 PSET7:SLEEP0:SLEEP200:PCLR7
1345 FOR Q = 1 TO 60: REM *WAIT 60 SECONDS*
1350 SLEEP0:SLEEP100
1355 NEXT Q
1360 NEXT S
1365 ASM&HBB,DB&H0E: REM *SET A/D CONVERTER POWER TO STAY ON*
1370 C=CHAN(0): REM *ENABLE A/D CONVERTER*
1375 PSET1: REM *TURN ON AMPLIFIER POWER*
1380 PSET7:SLEEP0:SLEEP200:PCLR7: REM *WATER PUMP*
1385 FOR R = 1 TO 60: REM *WAIT 60 SECONDS*
1390 SLEEP 0: SLEEP 100
1395 NEXT R

1470 REM **** DARK SIGNAL AVERAGES ****
1475 L = 0: M = 0: N = 0
1480 FOR R = 1 TO 65
1485 A = CHAN(3): B = CHAN(2): C = CHAN(1)
1490 L = L + A: M = M + B: N = N + C
1495 NEXT R
1500 L = L/65: M = M/65: N = N/65
1505 PRINT "DARK SIGNALS"
1510 PRINT #4,L," ",M," ",N
1515 K=L:V=M:W=N
1520 PRINT " "

1550 REM **** I AVERAGES ****
1555 PSET 0: REM *TURN LAMP ON*
1557 PSET7:SLEEP0:SLEEP200:PCLR7
1559 FOR R = 1 TO 60: REM *WAIT 60 SECONDS*
1561 SLEEP 0: SLEEP 100
1563 NEXT R
1565 PSET7:SLEEP0:SLEEP200:PCLR7: REM PULSE W-PUMP
1570 FOR R = 1 TO 20: REM *WAIT 20 SECONDS*
1575 SLEEP 0: SLEEP 100
1580 NEXT R
1595 T = 8: REM *NUMBER OF PTS TO AVERAGE*
1600 FOR Q = 1 TO T
1605 D = 0: E = 0: F = 0
```



```

1610 FOR R = 1 TO 65
1615 A = CHAN(3): B = CHAN(2): C = CHAN(1)
1620 D = D + A: E = E + B: F = F + C
1625 SLEEP 0: SLEEP 1. REM *DELAY BETWEEN DATA ACQS*
1630 NEXT R
1631 D = (D/65 - K): E = (E/65 - V): F = (F/65 - W)
1632 G = CHAN(7): REM *GET TEMPERATURE*
1633 G = TEMP(G): REM *CONVERT TO TEMPERATURE*
1636 RTIME
1637 PRINT D, " ", E, " ", F, " ", #4, G/100, " ", #02, ABS(G)%100, "
", #02, ?(2), " ", ?(1), " ", ?(0)
1643 REM @(Q) = D: @(Q+12) = E: @(Q+24) = F REM *ARRAY FOR STD DEV
CALC.*
1650 NEXT Q

1705 A = 0: B = 0: REM *GET BATTERY VOLTS*
1710 FOR R = 1 TO 10
1715 A = A + CHAN(4): B = B + CHAN(5)
1720 NEXT R
1725 PCLR 0: REM *LAMP OFF*
1730 A = A/10: B = B/10
1735 PRINT "BATTERY VOLTS ";
1740 PRINT #5, A, " ", B

1820 REM **** SHUT OFF AMPS, V SWITCHED ****
1825 FOR R = 0 TO 15 PCLR R: NEXT R: REM *CLEAR I/O*
1830 ASM &HBB, DB &H0A: REM *DISABLE A/D POWER*
1835 C = CHAN(0): REM *SHUT DOWN A/D CONVERTER*
1836 SLEEP 0: SLEEP 2400: REM *WAIT 24 SECONDS*
1838 RETURN

2000 REM ***** READ DATA FILE *****
2005 FOR Q = 1 TO (X/98)
2008 IF Q = 1 X = 0
2010 PRINT #02, "DETECTOR OUTPUTS @
", GET(X, #2), " ", GET(X, #2), " ", GET(X, #2);
2015 PRINT #02, " ", GET(X, #2), " / ", GET(X, #2), " / ", GET(X, #2)
2020 Y = GET(X, #2): A = GET(X, #2): B = GET(X, #2)
2025 PRINT "TEMP = ", Y, " A/D #1 = ", A, " A/D #2 = ", B
2030 A = GET(X, #2): B = GET(X, #2): C = GET(X, #2)
2035 PRINT #5, "CH434=", A, " ", "CH620=", B, " ", "CH740=", C
2040 A = GET(X, #2): B = GET(X, #2): C = GET(X, #2)
2041 PRINT #5, "CH434=", A, " ", "CH620=", B, " ", "CH740=", C
2042 A = GET(X, #2): B = GET(X, #2): C = GET(X, #2)
2043 D=A/4855: E=B/4855 REM *ANALOG TO VOLTAGE INTEGER
CONVERSION*

```

```

2044 A=A%4855 B=B%4855 REM *REMAINDER AFTER VOLTS CONVERSION*
2045 A=A*1000/4855 B=B*1000/4855 REM *DECIMAL VALUE OF
REMAINDER*
2046 IF A%10 >= 5 A= A/10 +1 GOTO 2048. REM *ROUND OFF TO 2 PLACES*
2047 A = A/10: REM IF 3RD PLACE <=5
2048 IF B%10 >= 5 B= B/10 + 1 GOTO 2050: REM *ROUND OFF TO 2 PLACES*
2049 B = B/10: REM *IF 3RD PLACE <=5*
2050 PRINT "BATTERY A = ", D, ".", A, " ", "BATTERY B = ", E, " ", B, " ", C
2052 PRINT " "
2053 PRINT " "
2055 SLEEP 0: SLEEP 10
2060 NEXT Q
2065 STOP
,

2999 REM *****
3000 REM ***** SET TATTLETALES TIME AND DATE *****
3005 REM
3010 INPUT 'ENTER THE YEAR (0 - 99) '(5)
3015 INPUT 'ENTER THE MONTH (1 - 12) '(4)
3020 INPUT 'ENTER THE DAY OF THE MONTH (1 - 31) '(3)
3025 INPUT 'ENTER THE DAY OF THE WEEK (1-7) 'Z
3030 INPUT 'ENTER THE HOUR OF THE DAY (0 - 23) '(2)
3035 INPUT 'ENTER THE MINUTE (0 - 59) '(1)
3040 INPUT 'ENTER THE SECOND (0 - 59) '(0)
3045 STIME
3050 REM ***** TRANSFER TIME AND DATE TO RTC *****
3055 RTIME
3060 PSET 10
3065 SDO &HB1,8: SDO &HB5,8: SDO &H00,8: REM *CCR & ICR SETUP*
3070 PCLR 10
3075 GOSUB 6000: REM CONVERT BINARY TIME TO BCD
3080 PSET 10: SDO &HA0,8: SDO ?(0),8: PCLR 10
3085 PSET 10: SDO &HA1,8: SDO ?(1),8: PCLR 10
3090 PSET 10: SDO &HA2,8: SDO ?(2),8: PCLR 10
3095 PSET 10: SDO &HA3,8: SDO Z,8: PCLR 10
3100 PSET 10: SDO &HA4,8: SDO ?(3),8: PCLR 10
3105 PSET 10: SDO &HA5,8: SDO ?(4),8: PCLR 10
3110 PSET 10: SDO &HA6,8: SDO ?(5),8: PCLR 10
3115 X = 0: REM ZERO MEMORY POINTER
3125 U = 0: REM ZERO BLANK CYCLE COUNTER
3130 GOTO 5
,

4000 REM ***** READ RTC & RELOAD TATTLETALE CLOCK *****
4005 PSET 10: SDO &H20,8: ?(0) = SDI(9): PCLR 10
4010 PSET 10: SDO &H21,8: ?(1) = SDI(9): PCLR 10
4015 PSET 10: SDO &H22,8: ?(2) = SDI(9): PCLR 10

```

```

4020 PSET 10: SDO &H23,8: Z = SDI(9): PCLR 10
4025 PSET 10: SDO &H24,8: ?(3) = SDI(9): PCLR 10
4030 PSET 10: SDO &H25,8: ?(4) = SDI(9): PCLR 10
4035 PSET 10: SDO &H26,8: ?(5) = SDI(9): PCLR 10
4040 GOSUB 7000: REM BCD TO BINARY CONVERSION ROUTINE
4045 RETURN

6000 REM ***** CONVERT BINARY TIME TO BCD *****
6005 RTIME
6010 FOR R = 0 TO 5
6015 @(R) = ?(R)/10: @(6) = ?(R)%10
6020 ?(R) = (@(R)*16) + @(6)
6025 NEXT R
6030 RETURN

7000 REM ***** CONVERT BCD TIME TO BINARY *****
7005 FOR R = 0 TO 5
7010 @(R) = ?(R)/16: @(6) = ?(R)%16
7015 ?(R) = (@(R)*10) + @(6)
7020 NEXT R
7025 STIME
7030 RETURN

8000 REM ***** ERROR TRAP FOR CLOCK *****
8010 ?(5) = 94
8015 ?(4) = 1
8020 ?(3) = 1
8025 ?(2) = 0
8030 ?(1) = 0
8035 ?(0) = 0
8040 Z = 7
8045 GOTO 3045: REM *CLOCK HAS BEEN RESET TO 1/1/94*
9000 REM ***** ERROR TRAP FOR MEMORY OVERFLOW *****
9005 IF X < 544402 GOTO 1000
9010 PSET 10
9015 SDO &HB2,8: SDO &H00,8: REM *ICR MODIFIED, ALARM DISABLED*
9020 PCLR 10
9025 FOR R = 0 TO 15: PCLR R: NEXT R
9030 DONE: REM *COMPLETE SYSTEM SHUTDOWN*

```

References

- BELLERBY, R. G. J., D. R. TURNER, G. E. MILLWARD, AND P. J. WORSFOLD. 1995. Shipboard flow injection determination of sea water pH with spectrophotometric detection. *Anal. Chim. Acta* **309**: 259-270.
- BOWER, V. E., R. G. BATES. 1955. pH values of the Clark and Lubs buffer solutions at 25°C. *J. Res. Nat. Bureau Standards* **55**: 197.
- BRICK, C. M. AND J. N. MOORE. 1996. Diel variation of trace metals in the upper Clark Fork River, Montana. *Environ. Sci. Technol.* **30**(6): 1953-1960.
- BYRNE, R. H. 1987. Standardization of standard buffers by visible spectrometry. *Anal. Chem.* **59**: 1479-1481.
- BYRNE, R. H. AND J. A. BRELAND. 1989. High precision multiwavelength pH determinations in seawater using cresol red. *Deep-Sea Res.* **36**(5): 803-810.
- CLAYTON, T. D. AND R. H. BYRNE. 1993. Spectrophotometric seawater pH measurements: total hydrogen ion concentration scale calibration of *m*-cresol purple and at-sea results. *Deep-Sea Res.* **40**(10): 2115-2129.
- COVINGTON, A. K. 1981. Recent developments in pH standardization and measurement for dilute aqueous solutions. *Anal. Chim. Acta* **127**: 1-21.
- COVINGTON, A. K., P. D. WHALLEY AND W. DAVISON. 1983. Procedures for the measurement of pH in low ionic strength solutions including freshwater. *Analyst* **108**: 1528-1532.
- DAVISON, W., AND C. WOOF. 1985. Performance tests for the measurements of pH with glass electrodes in low ionic strength solutions including natural waters. *Anal. Chem.* **57**: 2567-2570.
- DEGRANDPRE, M. D., M. M. BAEHR AND T. R. HAMMAR. 1999. Towards calibration-free optical chemical sensors. *Anal. Chem.* **71**: 1152-1159.
- DEGRANDPRE, M. D., T. R. HAMMAR, D. W. R. WALLACE AND C. D. WIRICK. 1997. Simultaneous mooring-based measurements of seawater CO₂ and O₂ off Cape Hatteras, North Carolina. *Limnol. Oceanogr.* **42**(1): 21-28.
- DEGRANDPRE, M. D., T. R. HAMMAR, S. P. SMITH AND F. L. SAYLES. 1995. In situ measurements of seawater pCO₂. *Limnol. Oceanogr.* **40**(5): 969-975.

- FUHRMANN, R., AND A. ZIRINO. 1988. High-resolution determination of the pH of seawater with a flow-through system. *Deep-Sea Research* **35**(2): 197-208.
- FULLER C. C., AND J. A. DAVIS. 1989. Influence of coupling of sorption and photosynthetic processes on trace element cycles in natural waters. *Nature* **340**(6228): 52-54.
- HAINES, T. A., J. J. AKIELASZEK, S. A. NORTON AND R. B. DAVIS. 1983. Errors in pH measurement with colorimetric indicators in low alkalinity waters. *Hydrobiologia* **107**: 57-61.
- HARBINSON, T. R. AND W. DAVISON. 1987. Performance of flowing and quiescent free-diffusion junctions in potentiometric measurements at low ionic strengths. *Anal. Chem.* **59**: 2450-2456.
- HARRIS, D. C. 1982. *Quantitative Chemical Analysis*, 2nd ed. W. H. Freeman and Company, New York, 92.
- HERCZEG, A. L. AND R. H. HESSLEIN. 1984. Determination of hydrogen ion concentration in softwater lakes using carbon dioxide equilibria. *Geochim. Cosmochim. Acta* **48**: 837-845.
- HERCZEG, A. L., W. S. BROECKER, R. F. ANDERSON, S. L. SCHIFF AND D. W. SCHINDLER. 1985. A new method for monitoring temporal trends in acidity of fresh waters. *Nature* **315**: 133-135.
- HOFFER-FRENCH, K. J. AND J. S. HERMAN. 1989. Evaluation of hydrological and biological influences on CO₂ fluxes from a karst stream. *J. Hydrol.* **108**: 189-212.
- KRATZ, T. K., R. B. COOK, C. J. BOWSER, AND P. L. BREZONIK. 1987. Winter and spring pH depressions in northern Wisconsin lakes caused by increases in *p*CO₂. *Can. J. Fish. Aquat. Sci.* **44**: 1082-1088.
- LEWIS, E., and D. W. R. WALLACE. 1998. Program developed for CO₂ system calculations. ORNL/CDIAC-105 Carbon Dioxide Information Analysis Center, Oak Ridge National Laboratory, U.S. Department of Energy, Oak Ridge, Tennessee.
- MABERLY, S. C. 1996. Diel, episodic and seasonal changes in pH and concentrations of inorganic carbon in a productive lake. *Fresh. Biol.* **35**: 579-598.
- MIDGELY, D. 1987. Assessment of reference electrodes for use in determining the pH of acidic, poorly-buffered waters. *Atmos. Environ.* **21**: 173-177.
- MILLERO, F. J. 1979. The thermodynamics of the carbonate system in seawater. *Geochim. Cosmochim. Acta* **43**: 1651-1661.

- MILLERO, F. J., R. H. BYRNE, R. WANNINKHOF, R. FEELY, T. CLAYTON, P. MURPHY AND M. F. LAMB. 1993. The internal consistency of CO₂ measurements in the equatorial Pacific. *Mar. Chem.* **44**: 269-280.
- PIA, S. H., D. P. WALTMAN, D. C. HILLMAN AND K. W. STREET, JR. 1990. Spectrophotometric determination of pH by flow injection. *Anal. Chim. Acta* **231**: 21-26.
- RAMETTE, R. W., C. H. CULBERSON AND R. G. BATES. 1977. Acid-base properties of tris(hydroxymethyl)aminomethane (tris) buffers in seawater from 5 to 40 °C. *Anal. Chem.* **48**: 867-870.
- RAYMOND, P. A., N. F. CARACO, AND J. J. COLE. 1997. Carbon dioxide concentration and atmospheric flux in the Hudson River. *Estuaries* **20**: 381-390.
- RONALD, L. 1999. unpublished data, University of Montana.
- ROBERT-BALDO, G. L., M. J. MORRIS, R. H. BYRNE. 1985. Spectrophotometric determination of seawater pH using phenol red. *Anal. Chem.* **57**: 2564-2567.
- STAUFFER, R. E. 1990a. Alkalinities of Maine lakes: are they really changing? *Limnol. Oceanogr.* **35**(6): 1238-1257.
- STAUFFER, R. E. 1990b. Electrode pH error, seasonal epilimnetic pCO₂, and the recent acidification of the Maine lakes. *Water Air Soil Pollut.* **50**: 123-148.
- WATERBURY, R. D., R. H. BYRNE, J. KELLY, B. LEADER, S. MCELLIGOTT AND R. RUSSELL. 1996. Development of an underwater *in-situ* spectrophotometric sensor for seawater pH. *SPIE* **2836**: 170-177.
- WEBB, J. A. AND I. D. SASOWSKY. 1994. The interaction of acid mine drainage with a carbonate terrane: evidence from the Obey River, north-central Tennessee. *J. Hydrol.* **161**: 327-346.
- ZHANG, H. AND R. H. BYRNE. 1996. Spectrophotometric pH measurements of surface seawater at in-situ conditions: absorbance and protonation behavior of thymol blue. *Marine Chemistry* **52**: 17-25.